Diseño y control de una microred en dc de baja tensión con recursos distribuidos de energía

Juan Sebastián Vélez Ramírez

Universidad Tecnológica de Pereira
Facultad de ingenierías
Maestría en Ingeniería Eléctrica
2021

Design and control of a low voltage dc-microgrid, with distributed energy resources

Juan Sebastián Vélez Ramírez

Final draft submitted as a partial requirement to obtain the title of:
M.Sc. in Electrical Engineering

Director:
Eduardo Giraldo Suárez, PhD.

Investigation group:
Control Automático

Universidad Tecnológica de Pereira
School of Engineering
Master in Electric Engineering
2021

Acceptance note

Jury

Jury

Jury

Pereira, 2021.

Acknowledgments

To my parents who have given me everything.

To my family and friends that gives light to my life.

With the purpose of envisioning other futures for humanity...

Motivation

The current global needs, demand drastic changes in the way we interact with our environment. Being the production of energy, the pillar that sustains the modern society, and also, the one that more contribute to the environmental damages that we now face. The need to reduce the use of fossil fuels, moves us towards a future with a growing electrical market, full of a diversity of loads such as electric vehicles, small industries, and homes [1, 2]. The challenges that climate change presents to humanity have motivated the investigation and development in renewable energies, a field with so many open issues. One of them is the problem of clustering and control distributed energy resources (DERs), like photo-voltaics (PV), wind-power (WP), and small hydro-power (SHP).

A micro-grid group loads and DERs in a single controllable entity, with clearly defined electrical boundaries. As a small scale power system, a microgrid can ensure self-supply and a considerable autonomy with respect to the grid, satisfying the needs of its network, bringing stability and reliability in the service, and isolating the loads from the grid failures. [3, 1, 4].

In the national context, Colombia's geographical location makes it one of the most vulnerable countries in terms of climate change, since its electricity generation network is composed mostly of hydroelectric power plants, a weak technology against droughts and phenomena such as *El niño*. However, the DERs deployment capacity available in the country, particularly in the Andes region, is virtually unlimited. In this aspect, the PV and SHP generation methods excel [5, 6]. In addition, with the growth of the country's energy demand, is estimated that by 2025 the total capacity must be increased by 60% [5]. In social terms, is well known that the high energy costs and the number of failures in remote sites, difficult the implementation of industrial developments in a little or middle scale. The lack of technology access for the rural population, makes the investigation and investment in the distributed generation, a need to achieve economic equity and overcome extreme poverty in the countryside.

Abstract

In this document a brief review of the DC microgrids generalities with emphasis in the control architecture is done. A novel hybrid-control architecture to take care of the inner, primary and secondary levels of DC microgrids monitoring, is simulated under different conditions. In the inner control architecture an **Modified Exact Feedback Linearization with integral action** approach, is proposed for control current or voltage in a Buck converter, designed to be part of the DC microgrid. The controllers are tested in simulation using Matlab-Simulink®. Results are compared with classic PID controllers and evaluated under two different mathematical tools (Mean Square Error, Integral Time Absolute Error) in order to prove their effectiveness. The evaluated data show that the proposed approach outperform the classical methods.

Different models of the said converters are clustered to build the microgrid scenario. Primary and secondary control architectures were designed in a centralized way with PI regulators of voltage and current. The microgrid was tested in Matlab-Simulink® with two disturbances, including a forced isolation of the microgrid, showing and acceptable performance.

0.1 Document structure

Chapter 1 enumerates the project objectives. In chapter 2 an introduction over the microgrids topic is done, considering state of the art in the distributed generators field, the differences between AC and DC distributions systems, and an introduction to the control architectures. Chapter 3 present the case study used to design the microgrid considering the generators topologies and the needs of the Colombian countryside. In chapter 4, the overall control architecture theory is described. Finally, chapters 5 and 6 present the results of the proposed controllers and the project's conclusions, respectively.

Contents

List of Figures

List of Tables

CHAPTER 1

Objectives

1.1 General objective

Design and control a low voltage DC microgrid powered by distributed energy resources.

1.2 Specific objectives

1. Research over the most suitable renewable DGs, their physical characteristics, dynamic models and control strategies.
2. Design a low voltage DC microgrid with the selected DGs and loads.
3. Design primary control strategies with a non-linear control technique and validate it through simulation.
4. Prove and validate primary and secondary control architecture in order to achieve acceptable voltage and current regulation.

CHAPTER 2

Introduction

2.1 Generalities of the microgrids

This section explores the main concepts involved in the microgrids investigation framework as well as general information relevant to the investigation process.

2.1.1 Distributed energy resources (DERs) and distributed generators (DGs)

Formally, a DER is any renewable or non-renewable energy source that, by means of small or medium-scale equipment, called DG, could produce electrical energy.Unlike the large power plants, the DGs are characterised by being located and distributed to guarantee the maximum exploitation of a region's energy resources; with low monetary and environmental costs, among other strengths.

The global electric market's projection foresees that by 2030, the 80% of the new installed capacity will come from fossil fuels, with all the environmental problems that this implies. Despite these forecasts, the concept of large power plants has been discussed through the DGs' high penetration in global networks. Also, the advent of DERs based on renewable technologies could help mitigate of the damages produced by the use of fossil fuels. [9].

In the technical field, the main impacts resulting from large-scale DGs integration are the voltage rise effect, power quality issues, branch overload problems, protection issues, and stability issues [10]. Tables 2.1 and 2.2 compares the principal DGs technologies and shows their differences in some remarkable aspects.

Technology	**Primary energy**	**Output type**	**Module power (kW)**	**Electrical efficiency (%)**	**Overall efficiency (%)**	**Advantages**	**Disadvantages**
Reciprocating engines	Diesel or gas.	AC	mar-00	30-43	$\sim 80-85$	• Low cost. • High efficiency. • Ability to use various.	• Environmentally unfriendly emissions.
Gas turbine	Diesel or gas.	AC	0.5-30000	21-40	$\sim 80-90$	Environmentally friendly. • Cost effective	• Too big for Small costumers.
Micro-turbine	Bio-gas propane or natural gas.	AC	30-1000	14-30	$\sim 80-85$	• Small size and light weight. • Easy start-up and shut down. • Low maintenance costs	• Expensive technology • Cost-effectiveness sensitive to the price of fuel. • Environmentally unfriendly emissions.
Fuel Cell	Ethanol, H2, N2, natural gas, phosphoric acid or propane.	DC	1-20000	05-55	$\sim 80-90$	• One of the most environmentally friendly generator. • Extremely quiet. • Useful for combined heat and electricity applications.	• Expensive infrastructure for hydrogen.

Table 2.1: Main non renewable DGs technologies [7].

Technology	**Primary energy**	**Output type**	**Module power (kW)**	**Electrical efficiency (%)**	**Overall efficiency (%)**	**Advantages**	**Disadvantages**
Wind-power	Wind	AC	0.2-3000	-	$\sim50-80$	• Day and night power generation. • One of the most developed renewable energy.	• Still expensive. • Need energy storage.
Photo-voltaic	Sun	DC	0.02-1000	-	$\sim40-45$	• Emission free. • usable in many applications	• Need energy storage. • High up-front cost.
Biomass gasification	Biomass	AC	100-20000	15-25	$\sim60-75$	• Minimal environmental impact. • Available throughout the world. • Alcohols and other fuels produced by biomass are efficient, viable, and relatively clean burning.	• Still expensive.
Small Hydro power	Water	AC	5-100000	-	$\sim90-98$	• Economic and environmentally friendly. • Relatively low up-front investment costs and maintenance. • Useful for providing peak power and spinning reserves.	• Suitable site characteristics required. • Difficult energy expansion. • Local environmental impact.
Geothermal	Hot water	AC	5000-100000	10-32	$\sim35-50$	• Environmentally friendly. • Low running costs	• No-availability of geothermal spots in the land of interest.
Ocean energy	Ocean waves	AC	10-10000	-	-	• High power density. • More predictable than solar or wind.	• Lack of commercial projects. • Unknown operations and maintenance costs.
Solar thermal	Sun and water	AC	1000-80000	30-40	$\sim50-75$	• Simple, low maintenance. • Operation costs nearly zero. • Developed technology.	• Unknown operations and maintenance costs. • Low energy density. • Limited scalability.

Table 2.2: Main renewable DGs technologies [7].

2.1.2 Energy storage systems (ESS)

The ESS are devices that can store energy in any of its forms, and deliver it as electrical power (current or voltage sources). The use of storage systems in microgrids is fundamental to ensuring power-sharing during fails and operational changes. Table 2.3 shows the most important technologies in this area.

Technology	**Efficiency** (%)	**Capacity** (MW)	**Energy Density** (Wh/kg)	**Capital** e/kW	**Lifetime (years)**	**Maturity**	**Environmental Impact**	**Examples**
TES	30-60	0-300	80-250	140-220	5-40	Developed	Small	Solar tow Central Receiver Solar Power Plant California (USA).
PHS	75-85	100-5000	0.5-1.5	400-1500	40-60	Mature	Negative	Rocky River PHS plant, Hartford(USA).
CAES	50-89	3-400	30-60	250–1500	20–60	Developed	Negative	Huntorf (Germany) and MacIntosh, Alabama(USA).
Flywheel	93-95	0-25	10-30	250	$\sim15	Demonstration	Almost	Commercially supplied by AFS-Trinity (USA), Beacon Power (USA), Piller (USA), etc.
Pb acid battery	70-90	0-40	30-50	200	5-15	Mature	Negative	BEWAG Plant, Berlin (Germany).
NiCd battery	60-65	0-40	50-75	350-1100	10-20	Commercial	Negative	Golden Valley, Alaska USA.
Li-ion battery	85-90	0-1	75-200	3000	5-15	Demostration	Negative	Kyushu Electric Power and Mitsubishi Heavy Industries (Japan).
Fuel Cells	20-50	0-50	800-10000	350-1100	5-15	Developing	Small	Topsoe FuelCell, Lyngby, (Denmark).
Flow battery capacitors	75-85	0.3-15	10-50	400-1100	5-15	Developing	Negative	Innogys Little Barford Power Station, (UK).
Capacitors	60-65	0-0.05	0.05-5	250	$\sim5	Developing	Small	Commercially supplied by SAFT (France), NESS (Korea), ESMA(Russia) etc.
Supercapacitors	90-95	0-0.3	2.5-15	200	> 20	Developed	Small	PowerCache (Maxwell,USA), ELIT(Russia), PowerSystemCo. (Japan), Chubu Electric Power (Japan), etc.
SMES	95-98	0.1-10	0.5-5	200	>20	Demonstration	Positive	Wisconsin Public Service Corporation (USA).

Conventions:
TES: Thermal energy storage.
PHS: Pumped hydro storage.
CAES: Compressed sir energy storage.
Pb-acid battery: Lead-acid battery.
Ni-Cd battery: Nickel-cadmium battery.
Li-ion battery: Lithium-ion battery.
SMES: Superconduction magnetic energy storage.

Table 2.3: Main ESS technologies [7].

2.1.3 Power electronics converters

The central operation systems of a microgrid, are the power electronics converters. With appropriated control algorithms, these devices enable the transformation of different forms of electric energy (DC and AC of high and low voltage). The most used power converters topologies are different variants of the classical converters, as the Buck, Buck-Boost and Boost, that can be mono-directional or bi-directional depending of the controlled DG; and the implementation of cascade voltage source converters (VSC) in DC-AC or AC-DC applications.

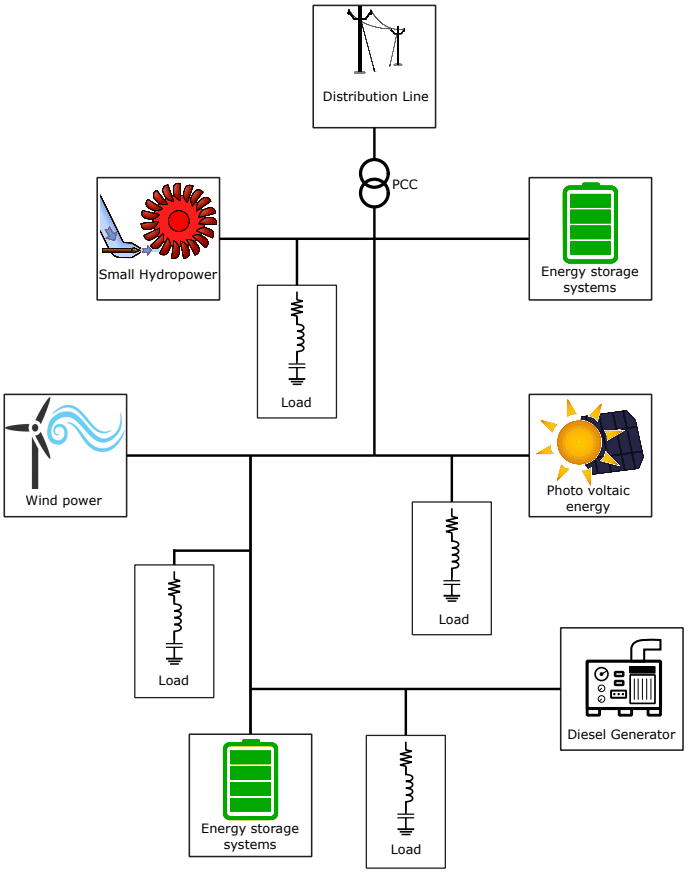

Figure 2.1: Example of a microgrid with distributed energy resources.

2.1.4 Microgrid definition

In the discussion about the new distribution systems topologies, the integration of the non-conventional energy resources, and the standardization of the so-called *smart grid*, the microgrid concept has won special attention due to the flexibility, reliability, and benefits that these network topologies will add to the distribution lines in the near future [9].

Several definitions have been established for a microgrid, and each country has legislation about the grid features, and its operational capabilities. In general, all definitions agree that a microgrid is a cluster of distributed generators and loads, with clearly defined electrical boundaries and the capacity of operating in connection with the grid or autonomously (island mode) [2, 3, 1]. According with these definition, Fig. 2.1 shows an arbitrary microgrid architecture with distributed generators and loads.

A relevant characteristics of every microgrid is the Point of common coupling abbreviated PCC, in which the system interacts with the utility grid, and the inte-

gration of several distributed generators.

2.2 DC vs AC

The first known microgrid was made by Thomas Edison in 1882, when he installed 50 small scale power plants in a course of four years [1]. But, as a concept, the word *microgrid* was introduced by professor R.H Lasseter of university of Wisconsin-Madison in 2001. This year is the beginning in the investigation on the microgrid field. [1], [2]. Multiple laboratories and test facilities were deployed around the world during this period, some of the most important were located in Greece, United States, Italy, England, Japan and China.

The development of microgrids around the world revive the old battle between the two modes of electric energy distribution (AC and DC). This, due to the advances in the power electronics converters field and the developments in the microgrids deployment, leading the integration of new generation technologies. Microgrids topologies are now divided between AC and DC operation modes. Has been proved that the implementation of DC-based microgrids, will transform the way of the energy management; specially, in the fields of transport, telecommunications, informatics and industry. This, due to the design and control simplicity, and efficiency compared to AC microgrids [4], [8]. Differences between these two technologies can be seen in table 2.4.

Influence parameter	**AC distribution line**	**DC distribution line**
Power transmitted	Less efficiency due to high line loss, hence less power transmission. Require more conductors	More efficiency and more power transmission. Require few conductors
System stability	Less stable due to easily affected by external disturbances	More stable and can also increase the stability of the AC microgrid systems.
Reluctance	Have reactance in line	No reactance in the line and hence more power transmitted
Frequency (50 Hz or 60 Hz	Frequency monitoring is mandatory	Frequency is zero, so no need of frequency monitoring
Resistance	High line resistance and hence high losses	Have low line resistance and hence low line losses.
Susceptance	Charging current and over-voltage problem lead to high cost and low power transmission.	Do no exist, and hence effect of over-voltage and over-charging leading and high power transmission.
Analysis	Involve complex numbers and hence difficult to analyze.	Involve only real number i.e more simple.

Table 2.4: Comparison between AC and DC distribution lines [8].

Table 2.5 compare research results in the control aspect of AC and DC microgrids.

Operating mode	AC microgrids	DC microgrids
Grid-connected Mode		
MGCC	• Monitoring system diagnosis by collection information from the LVAC network, DGs units and loads (AC and DC). • Performing state estimation and security assessments, evaluate economic generation scheduling active and reactive power control of the DGs units and demand side management function using the available information. • Ensuring synchronized operation with the main grid, maintaining the power exchange at prior contract points.	• The main function of the MGCC is to independently control the power flow and load-end voltage profile of the DC units in response to any disturbance and load changes. • Participation in economic generation scheduling, load tracking or management and demand side management (DSM) by controlling the storage devices.
DGCS	• Ensuring that each DG unit rapidly picks up its generation to supply its share of the load in stand-alone mode and comes back to the grid connected mode automatically with the help of the MGCC	• Ensuring that each DG unit quickly picks up its generation to supply its share of the load in stand-alone mode and comes back to the grid connected mode automatically with the help of MGCC.
Island mode		
MGCC	• Performing active reactive power control of the DGs in order to maintain stable voltage and frequency at the load ends. • Managing load interruption/shedding strategies using demand side management (DSM) with ESS support for maintaining power balance and voltage. • Initializing local black start to ensure reliability and continuity of the service. • Switching the microgrid to grid-connected mode after the main grid supply is restored without hampering the stability.	• Independently control the power flow and load-end voltage profile of the DG units in response to any disturbance and lad changes. • Ensuring the DG units rapidly pick ups its generation to supply its local load islanding mode and automatically reconnect to grid with the help of the MGCC.
DGCs	• Commanding each DG unit to rapidly pick up this generation to supply its corresponding local in the stand-alone mode and automatically re-synchronize to grid with the help of the MGCC.	• Ensuring that each DG unit rapidly picks up this generation to supply this share of the load in stand-alone mode and comes back to the grid-connected mode automatically with the help of the MGCC.

Conventions:
MGCC: Microgrid central controller.
LVAC: Low voltage AC network.
DGCS: Distributed generator control system

Table 2.5: Comparison between AC and DC control tasks [8].

Accurate, actualised and detailed information about the state of art in microgrids control is provided in [11], [12] and [13].

With a exhaustive revision of the literature, is possible to conclude that DC microgrids have a considerable advantage against AC microgrids.

2.3 Introduction to DC microgrids control strategies

The growing of the distribution generation, makes the control structure a fundamental axes of the microgrids operation. The main control objectives are given below.

- Efficient voltage and current control in every operating mode.
- Proportional load sharing.
- Stable operation with constant and non-linear loads.
- Coordination among different DERs and ESS.
- Synchronisation with the utility grid.
- Power flow control within DC microgrid and the utility grid.
- Smooth transition between grid-connected to island mode.

Different control task are required by an MG in order to satisfy the objectives above. The main control challenges in this field arise from the unknown behaviours of the renewable sources such as photo-voltaic and wind-power.

Usually, the control of microgrids is designed according to the structure depicted in Fig. 2.2, in which each layer seeks to meet specific control objectives, determined by the system's operational needs. The primary layer (field level) takes care of the internal control of each distributed generator and loads, regulating the power production and loads consumption. The secondary layer (management level) seeks to maintain the grid's stable operation, exchanging information with the tertiary layer to set the appropriate references to the first layer. In the end, the tertiary layer (grid level) regulates the economic dispatch, determining the times to sell or buy energy from the utility grid and the charge or discharge of energy storage nodes [7, 14, 15].

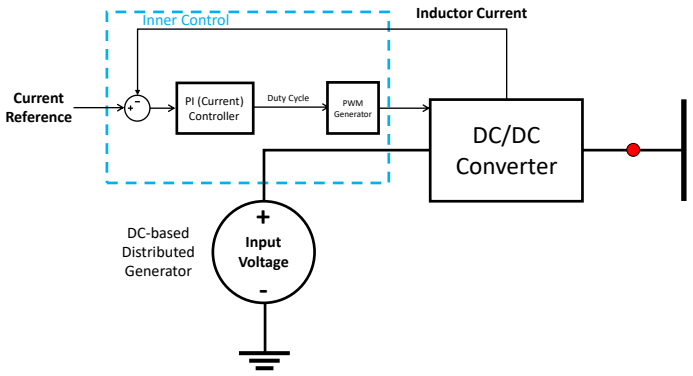

Figure 2.3: Classic current PI controller in power electronic devices.

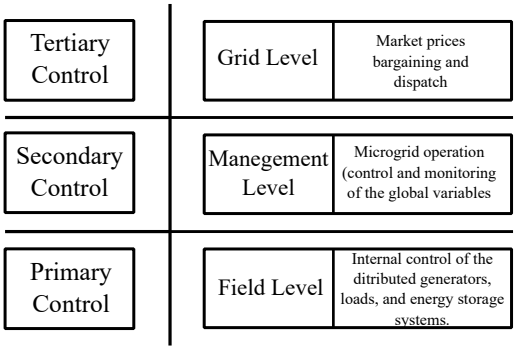

Figure 2.2: Hierarchical control structure in a microgrid [7].

2.3.1 Internal control

Most of the literature refers the internal control as a part of the primary control strategies, since it must be located internally in the DG or load interfaces, with the objective of control the primary variables of the power electronic converter. For explanatory purposes, a separation of the internal and primary controllers is made in this research.

A PI controller is applied with current feedback in classical architecture to track a reference current as is depicted in Fig. 2.3.

To control the output voltage, over the current loop in Fig. 2.3, is implemented a PI outer loop with an output voltage feedback, as is shown in Fig. 2.4, this is known as voltage-current cascade control.

PI controllers are simple and with relative easy tuning. This research proposes a non-linear control technique that has better response and better sturdiness against perturbations. The detailed explanation is developed in chapter 4.

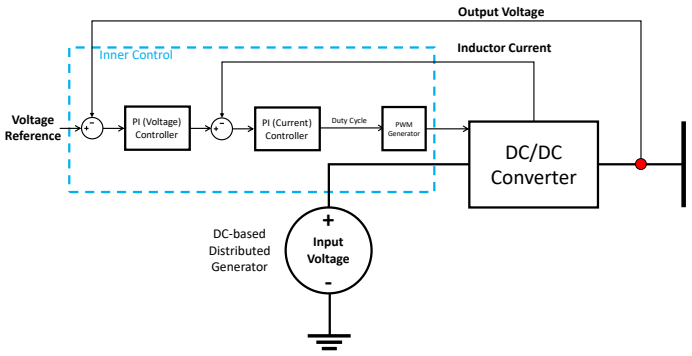

Figure 2.4: Classic voltage cascade PI controller in power electronic devices.

2.3.2 Primary control strategies

In the field level, the conventional controller implemented is the droop control. In DC microgrids the power is proportional to the current, and hence both, voltage and current, can be used to implement the droop controller [16, 17, 18]. Detailed explanation about this control architecture is available on chapter 4.

2.3.3 Secondary control strategies

The microgrid's main control objectives are performed in the second layer. These control objectives include the turn-on, the turn-down, isolation, and re-connection protocols, besides the regulation of the internal power production and consumption [10]. The control architecture in this layer does not have a consensus due to the different topologies proposed in the literature. These are the centralized, distributed, and decentralized methods, [17, 14, 19].

Centralized control

The centralised control uses an overall communication system ruled by a Microgrid central controller (MGCC) usually located at the PCC. Generally, it gives better performance throughout optimising the system by collecting all required information in one single algorithm driven by the central processor.

Due to the better performance and efficiency, the centralized control has lead to significant developments in optimization and robustness, as is shown in [20, 21], and the coordination of different renewable sources power dispatch shown in [22]. Notwithstanding, as demonstrated in [23, 17], a significant issue that centralized architecture has, is the single point failure, since the central controller carries out all the microgrid operations, a fail in this point will lead to a generalized system collapse; also this kind of controller lacks of scalability, which hinders the growth of the microgrid, associated with the integration of new DGs and loads.

Decentralized control

The decentralised control methods operates based on local information, observed by each node of the microgrid, this guarantee the free connection of new nodes.

Examples of decentralized controllers whit significant improvements could be seen in [24, 25], with a robust drop control strategies in [24], and a sliding mode control in [25]. A well-known drawback of the decentralized control, also developed by [23] is the poorer energy and frequency quality (compared with centralized structures) to the time delays among the controller's response; this strategy also have to overcome problems of communication derived of the noise injected in the digital buses by the power lines, and issues in the regulation of voltage and load sharing. [26],[27].

Distributed control

The distributed strategies seek to obtain the best features of both architectures: the improved variable management of the centralized, and the flexibility and plug and play service of the decentralized. The literature in distributed topologies includes complex methodologies like H_∞ norm, model predictive control (MPC), and intelligent control, among others, all have in common model-based math techniques and complex implementation to the algorithms computational cost. In [28] an MPC technique is applied to a renewable-based microgrid with satisfactory results. In [29] a novel *broadcast gossip technique* with applicability in real-world scenarios is presented. In [30], a resilient distributed control with the capability of avoiding certain sensor faults is shown.

CHAPTER 3

Design of a low voltage DC microgrid

This chapter present the design criteria of a small scale microgrid, taking as a reference, the project that served as inspiration to carry out this research.

3.1 Distributed generators classification

According to its utility, every DG could be divided in dispatchable and non-dispatchable units. Dispatchable units can be controlled to provide the necessary power to maintain the grid stability, non-dispatchable units only deliver a specific amount of power according to the actual capacity of the associated DER. Three variations of these divisions can be considered [19]:

3.1.1 Grid forming/supporting node

With a classical control scheme depicted in Fig. 2.4, a dispatchable unit could work as grid forming or grid supporting node. The grid forming node assume the role of *master* of the microgrid, setting the voltage reference of the DC-link; in grid connected mode, usually this role is carried out by the utility grid. A grid supporting node, set the voltage to its neighborhood, supporting the grid forming node; in island operation, all the supporting nodes must work together to maintain stability in the microgrid, this is called *Cooperative control*. A simplified model of grid forming/supporting node is depicted in Fig. 3.1-(a).

3.1.2 Grid feeding node

The control scheme shown in Fig. 2.3 is normally implemented in non-dispatchable units called grid feeding nodes. With a maximum power point tracking (MPPT),

like the developed by Ospina [31], these sources only inject power o current to the DC-link. A simplified model of grid feeding nodes is presented in Fig. 3.1-(b).

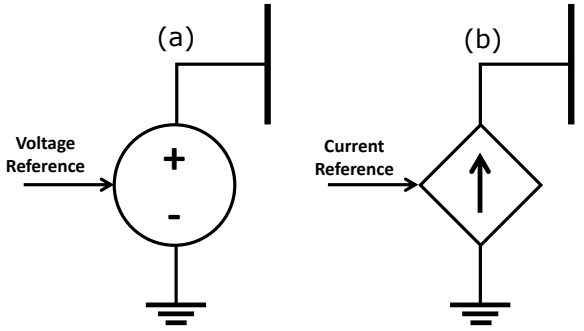

Figure 3.1: Simplified microgrid nodes. (a) Grid forming/supporting node. (b) Grid feeding node.

3.2 Case study: Intensive fish farming project

3.2.1 Generalities

An intensive fish farming project is an automated food production project, in which the final product is fresh fish. Differs of the traditional fish farms in crucial aspects: the production volumes, the level of automation, and the energy consumption.

The main aspect of this kind of developments is the production area. In a small area, a well deployed intensive fish farm, could produce, near six or seven times the same amount of fish that a traditional farm with same extension. This is only possible with the implementation of an aeration system that allows bigger fish concentrations in a smaller space. The aeration system must operate 24 hours, 7 days a week, because if it stops will lead to the loss of all production. However, the constant use of electro-mechanical aireators is a considerable load to handle with. Other loads that must to be taken into account are: illumination and general porpoise sockets, an electric pump, and an industrial freezer.

More information about the issues related to this projects are available in references [32, 33, 34]

3.2.2 APISBAL project

Fig. 3.2 refers the location and geography of the project developed by the APISBAL association.

With an estimated production of 1 ton per month, the project is considered small. However, about 10 rural families depend on the success of the project.

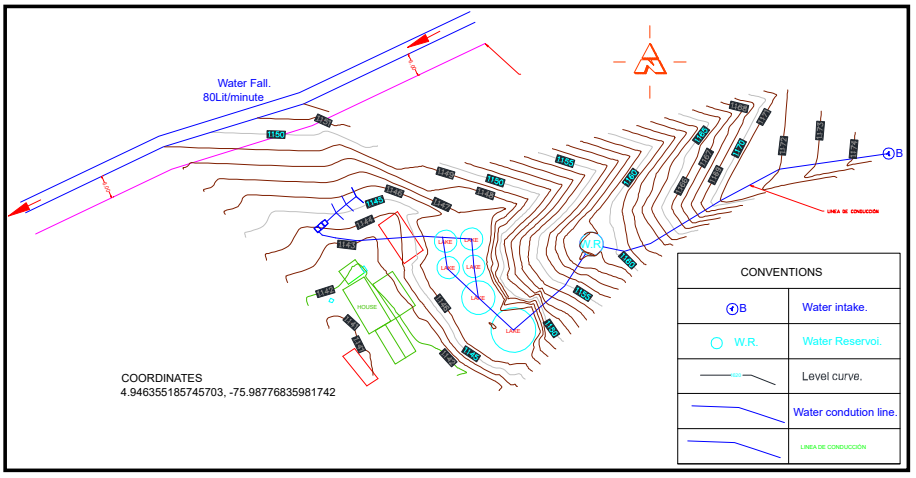

Figure 3.2: Project location map.

The total load calculated is shown in table 3.1. This information is a basis of the microgrid design.

Element	Nominal power (Watts)
Variable-frequency drive	7500W
Electric pump	1500W
Other loads	1900W
Total	10900W

Table 3.1: Main loads of the fish farm project.

3.3 Proposed design

Fig. 3.2 shows a near water fall that can sustain an SHP plant. This kind of DG is optimal to be implemented as a grid supporting node.

Additional information can be obtained of the *Global solar atlas* provided by *The world bank* [35]. With the location coordinates is possible to determine that the full sun hours (FSH) annually are approximately of $1680h/y$, which is an optimal value to deploy PV arrays. PV generation, as a renewable source is suitable to be a grid feeding node in a microgrid.

Every microgrid needs an energy supply system, the battery energy storage (BES) is the best solution in this kind of projects. Due to the size of the battery bank, BES has better operation as a grid feeding node.

Suggested nominal power of each node is available on table 3.2. These values were estimated having in account the variability of SHP and PV sources, and the possibility of a **net metering** exchange with the utility grid.

Node	Nominal Power
SHP	$9500W$
PV	$7600W$
ESS	$5700W$

Table 3.2: Suggested nominal power of the DGs nodes.

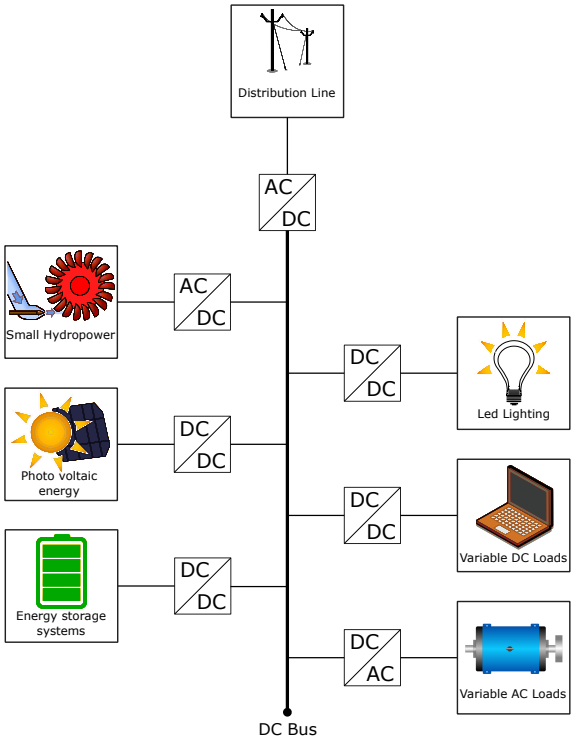

Figure 3.3: Simplified microgrid design to the fish farm project.

With this information is easy to propose a simple DC microgrid design that can handle the local loads in connection with the utility grid. Fig. 3.3 shows the one-line diagram of the proposed microgrid.

In terms of reliability this kind of microgrid might have energy losses due to the variability of the renewable sources. This model could be improved with the inclusion of a diesel generator.

CHAPTER 4

Hierarchical control in a DC microgrid

This chapter explores the theoretical and mathematical background related to the microgrid control levels from the internal converter control to the secondary level.

4.1 Inner control

This chapter references are supported in [36].

The constant search for more robust primary level controllers has become a relevant field of investigation in the state of the art of DC distribution systems. The Buck converter has been widely studied in recent years due to its simplicity, reliability, and relatively low construction cost, which make it suitable to be part of every DC microgrid. Being a reducer-type converter, in exchange for the difference between input and output voltages, the Buck converter can handle higher output currents than the input equivalent [37]. These facts make it suitable to be located in the load-side, controlling voltage, current or power of led-based illumination systems, internet servers, industrial automation arranges, and other DC loads.

As said above, a Buck converter integrated into a microgrid must have a robust controller with the capability to operate over contingencies and disturbances like changes in the input voltage or the load size. This capability is required to improve the whole system performance. The Exact Feedback Linearization (EFL) is a non-linear control technique that searches for a linear transformation of non-linear systems. The objective is to construct a control signal that can eliminate nonlinearities' effects on the dynamic system's behavior [38, 39].

4.1.1 The Buck Converter

In Fig. 4.1, the classic electrical structure of a buck converter is shown, where E is the input voltage, μ is the boolean control signal that activates the electronic switch (usually a MOSFET or IGBT transistor), i is the inductor current, and v is the output voltage.

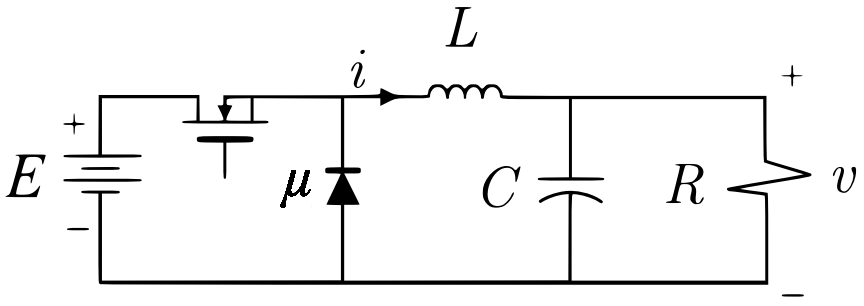

Figure 4.1: General structure of a Buck converter.

The constants of the model that define its operation characteristics are the inductance L in Henrys, the capacitance C in Farads, and the load resistance R in Ohms.

Design

The design of a converter depends on its application. In this case, it must be part of a DC microgrid with a structure, as shown in Fig. 3.3. The Buck converter could be connected to the DC bus, feeding the led lighting system or the variable DC-load node.

In terms of the design criteria, the most used switching strategy is the known pulse width modulation (PWM), in which the energy of the input voltage is managed by the time of the "On" state of the switch. In Fig. 4.2 is shown the behavior of the diode voltage during the PWM signal period (T).

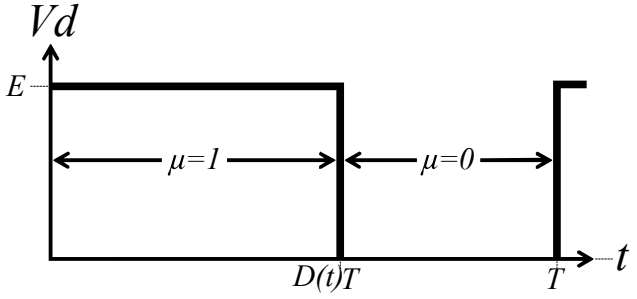

Figure 4.2: Waveform of the diode voltage in period T of the PWM.

This lets the introduction of the duty cycle variable ($D(t)$), as a percentage of T, that can be expressed along with μ as presented in (4.1).

$$\mu = \begin{cases} 1; & 0 \leq t \leq D(t)T \\ \\ 0; & D(t)T < t \leq T \end{cases} \tag{4.1}$$

Equation (4.1) can be simplified in terms of D giving (4.2).

$$\mu = \begin{cases} 1 & D(t) \\ \\ 0 & (1 - D(t)) \end{cases} \tag{4.2}$$

With this, it is possible to calculate the critical inductor and capacitor in terms of a continuous conduction mode of operation.

$$L_c = \frac{(1-D^*)R}{2f}; \quad C_c = \frac{1-D^*}{16L_c f^2} \tag{4.3}$$

where f is the switching frequency related to the switching period by expression (4.4), and D^* is the nominal value of the duty cycle in the equilibrium point. Being f defined as:

$$f = \frac{1}{T} \tag{4.4}$$

being T the time between two consecutive rising flanks.

With the above set of equations is possible to design a standard Buck converter in continuous conduction mode. It is important to note that E and R are taken theoretically as constants, but they are subject to disturbances that test the control's robustness in practice.

Dynamic model

To obtain a proper dynamic model is a need to understand the input signal yield's behaviors in the system.

Let be the input $\mu = 1$. Then, Fig. 4.1 neglecting power losses, can be simplified as shown in Fig. 4.3.

Defining the states of the new system (i,v), the differential equation that model its behavior in function of the time are (4.5).

$$L\frac{di}{dt} = E - v(t) \tag{4.5a}$$

$$C\frac{dv}{dt} = i(t) - \frac{1}{R}v(t) \tag{4.5b}$$

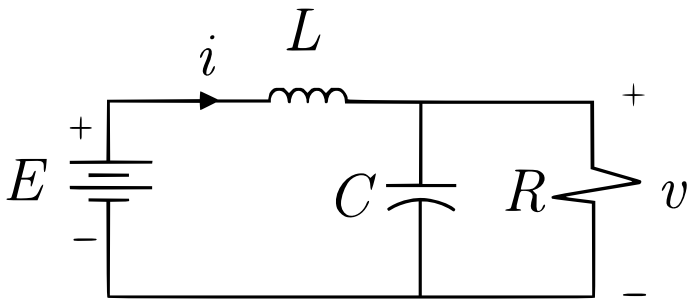

Figure 4.3: Buck converter when $\mu = 1$, neglecting power losses.

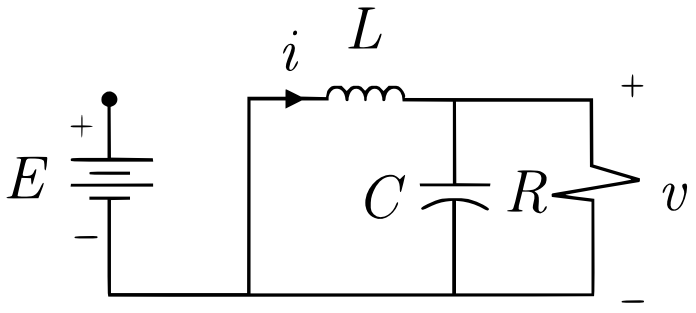

Figure 4.4: Buck converter when $\mu = 0$, neglecting power losses.

Now, let be $\mu = 0$. The new schematic of the converter could be simplified as shown in Fig. 4.4

And the resulting differential equations are shown in (4.6), as follows:

$$L\frac{di}{dt} = -v(t) \tag{4.6a}$$

$$C\frac{dv}{dt} = i(t) - \frac{1}{R}v(t) \tag{4.6b}$$

The sets (4.5) and (4.6) depend exclusively on the state of the input signal μ. Multiplying (4.2) by both expressions respectively, the set (4.5) becomes (4.7).

$$L\frac{di}{dt} = \Big(E - v(t)\Big)D(t) \tag{4.7a}$$

$$C\frac{dv}{dt} = \left(i - \frac{1}{R}v(t)\right)D(t) \tag{4.7b}$$

The same procedure is performed with the set (4.6), resulting in (4.8).

$$L\frac{di}{dt} = -v(t)\Big(1 - D(t)\Big) \tag{4.8a}$$

$$c\frac{dv}{dt} = \left(i - \frac{1}{R}v\right)(1 - D(t)) \tag{4.8b}$$

Finally, equations (4.7) and (4.8) are added in order to create an averaged model of converter, as presented in (4.9).

$$L\frac{di}{dt} = ED(t) - v(t) \tag{4.9a}$$

$$C\frac{dv}{dt} = i(t) - \frac{1}{R}v(t) \tag{4.9b}$$

The pack of equations (4.9) could be expressed in state space, as shown in (4.10).

$$\begin{bmatrix} \dot{x_1} \\ \dot{x_2} \end{bmatrix} = \begin{bmatrix} 0 & -\frac{E}{L} \\ \frac{1}{C} & -\frac{1}{RC} \end{bmatrix} \begin{bmatrix} x_1 \\ x_2 \end{bmatrix} + \begin{bmatrix} \frac{E}{L} \\ 0 \end{bmatrix} \Delta u \tag{4.10}$$

With (4.9) and (4.10) it is possible to introduce the different control strategies implemented below.

Behavior analysis

Calculation of the transfer function throw essential facts about the dynamic response of the converter's state variables. By applying the Laplace transform to (4.9) and building the equivalent transfer functions of current (4.11) and voltage (4.12), it is possible to analyze some facts that guarantee the performance of the non-linear controllers.

$$I(s) = \frac{\left(\frac{E}{L}s + \frac{E}{LCR}\right)D(s)}{s^2 + \frac{1}{RC}s + \frac{1}{LC}} \tag{4.11}$$

$$V(s) = \frac{\frac{E}{LR}D(s)}{s^2 + \frac{1}{RC}s + \frac{1}{LC}} \tag{4.12}$$

One remarkable thing about the Buck converter is the zero location of both of the transfer functions. Unlike other kinds of converters like the Boost or the Buck-Boost, the Buck does not present zeros located on the positive side of the complex plane for both transfer functions. This means that it is a minimum-phase system, so the voltage and current have stable inner dynamics [31, 38]. Replacing

the parameters of table 5.1 in (4.11) and (4.12), is possible to get the poles and zeros values of both transfer functions.

Current transfer function is depicted in Fig. 4.5, and have a zero located in the negative side of the complex plane.

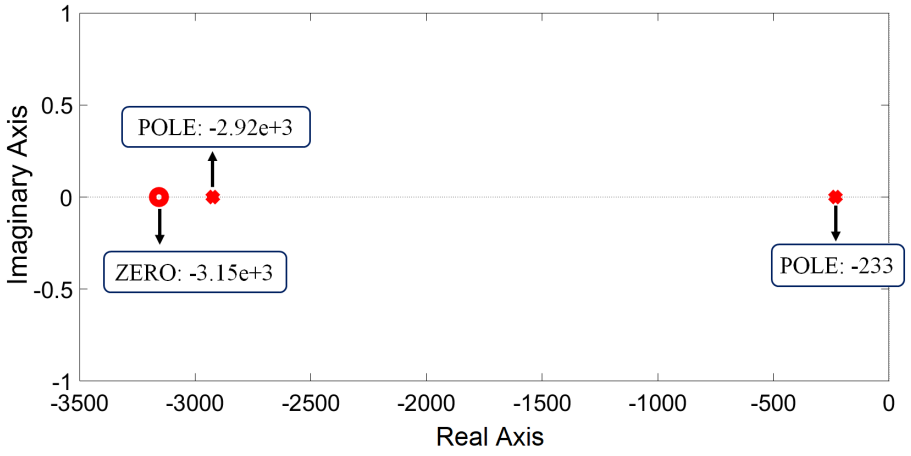

Figure 4.5: Poles and zeros locations of the current transfer function.

Voltage transfer function has two poles and does not have zeros, as presented in Fig. 4.6.

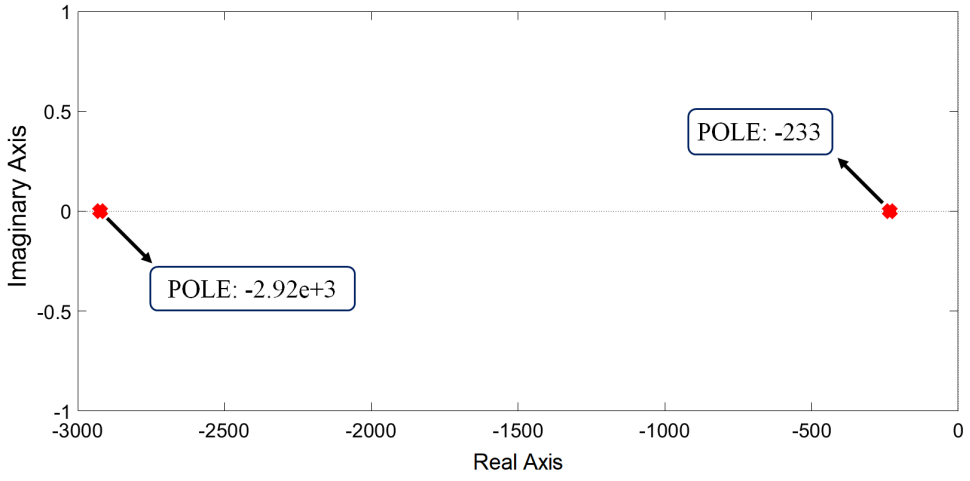

Figure 4.6: Poles and zeros locations of the voltage transfer function.

This is a key to develop the EFL controllers since the order stability of the internal dynamic determines the designed control law's applicability. It can be concluded that both state variables: current, and voltage, have stable inner dynamics, so that an EFL technique could be proposed for each one [39].

4.1.2 Modified Feedback linearization with integral action to control current and voltage

The generalized model of a nonlinear dynamic system is given by (4.13)

$$\dot{x} = f(x) + g(x)u(t) \tag{4.13}$$

A nonlinear state space model, where $x(t)$ is a vector that contains the state variables, and $f(x)$ and $g(x)$ are independent functions of x.

The set of equations of (4.9) can be transformed into state space model giving (4.14).

$$\dot{x_1} = \frac{E}{L}D(t) - \frac{1}{L}x_2(t) \tag{4.14a}$$

$$\dot{x_2} = \frac{1}{L}x_1(t) - \frac{1}{RC}x_2(t) \tag{4.14b}$$

where x_1 is the inductor current (i) and x_2 is the output voltage (v).

Current control

By defining the output of the system as $x_1(t)$, as is shown in (4.15).

$$y(t) = x_1(t) \tag{4.15}$$

The derivative of this equation is given by (4.16).

$$\dot{y}(t) = \dot{x_1} = \frac{E}{L}D(t) - \frac{1}{L}x_2(t) \tag{4.16}$$

In this case, for current control, the output of a second-order system appears in the first derivative, throwing a reduced-order control. This is not a problem since it was demonstrated that the current inner dynamics are stable. Thus, equation (4.16) can be compared to a corrective function Ψ as shown in (4.17).

$$\dot{x_1} = \Psi \tag{4.17a}$$

$$\frac{E}{L}D(t) - \frac{1}{L}x_2(t) = \Psi \tag{4.17b}$$

Defining $e(t)$ as the error (4.18), the following equation is obtained:

$$e(t) = x_1(t) - x_{1d}(t) \tag{4.18}$$

where $x_{1d}(t)$ is the reference. The function Ψ can be defined to guarantee a reference tracking, with a proportional gain K and an integral action that ensures the error correction, adjusting the value of the integral gain K_i. Resulting Ψ is (4.19).

$$\Psi = -Ke(t) + K_i e_i(t) \tag{4.19}$$

where $e_i(t)$, known as the integrative error, is defined as:

$$e_i(t) = \int_0^t e(\tau)d\tau \tag{4.20}$$

By applying derivatives at both sides of expression (4.20), the expression (4.21) is obtained.

$$\dot{e_i} = e(t) = x_1(t) - x_{1d}(t) \tag{4.21}$$

A new closed-loop state space model can be built from the first order differential equations (4.17) and (4.21), as shown in (4.22).

$$\begin{bmatrix} \dot{x_1} \\ \dot{e_i} \end{bmatrix} = \begin{bmatrix} 0 & 0 \\ 1 & 0 \end{bmatrix} \begin{bmatrix} x_1 \\ e_i \end{bmatrix} + \begin{bmatrix} 1 \\ 0 \end{bmatrix} \Psi - \begin{bmatrix} 0 \\ 1 \end{bmatrix} x_{1d} \tag{4.22}$$

And the control law that guarantee the reference tracking is given by (4.23), as follows:

$$D(t) = \left(-Ke(t) + K_i e_i(t) + \frac{1}{L} x_2(t) \right) \frac{L}{E} \tag{4.23}$$

Since the input voltage E is a non-controlled input instead of a constant, and for microgrids applications, must be a global variable available for all the primary level controllers, then the feedback of E ensures a fast response against changes in the main DC bus. This guarantees the operation of the node.

Fig. 4.7, shows a simplified schematic, in which the control law of (4.31) is embedded in the the inner control block.

Voltage control

Unlike other standard converters, the Buck does not present unstable behaviors in the voltage loop side, this means that an EFL procedure can be developed. Lets define the voltage as the output of the system. In order to guarantee a linear transformation of the model, a new space must be defined, lets call this as the vector $z(t)$.

$$y(t) = x_2(t) = z_1(t) \tag{4.24}$$

The first derivative of (4.24) is given by (4.25).

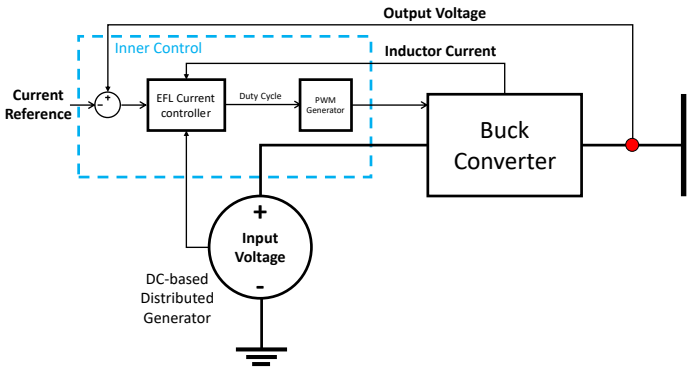

Figure 4.7: EFL current control schematic.

$$\dot{z_1} = -\frac{1}{RC}x_2(t) + \frac{1}{C}x_1(t) = z_2(t) \tag{4.25}$$

Since the control signal D doesn't exist in the first derivative, the second derivative must be calculated. The resulting expression contains the control signal so it can be equalized to the corrective function Ψ as shown in (4.26).

$$\dot{z_2} \quad = \quad -\frac{1}{RC}x_1(t) \quad + \quad \left(\frac{1}{(RC)^2} - \frac{1}{LC}\right)x_2(t) \quad + \quad \left(\frac{E}{LC}\right)D(t) \quad = \quad \Psi \tag{4.26}$$

The corrective function Ψ is designed for a complete order model. By adding the integral action, the expression (4.27) is obtained.

$$\Psi = -K_1 z_1(t) - K_2 z_2(t) + K_i e_i(t) \tag{4.27}$$

where the error is given by (4.28),

$$e(t) = x_2 - x_2 d \tag{4.28}$$

And the integrative error e_i given by (4.29)

$$e_i(t) = \int_0^t e(\tau)d\tau \tag{4.29}$$

The augmented state space model is presented in (4.30), as follows:

$$\begin{bmatrix} \dot{z_1}(t) \\ \dot{z_2}(t) \\ \dot{e_i}(t) \end{bmatrix} = \begin{bmatrix} 0 & 1 & 0 \\ 0 & 0 & 0 \\ 1 & 0 & 0 \end{bmatrix} \begin{bmatrix} z_1(t) \\ z_2(t) \\ e_i(t) \end{bmatrix} + \begin{bmatrix} 0 \\ 1 \\ 0 \end{bmatrix} \Psi - \begin{bmatrix} 0 \\ 0 \\ 1 \end{bmatrix} x_2 d \tag{4.30}$$

Clearing $D(t)$ from expression (4.26) the model's control law is given (4.31).

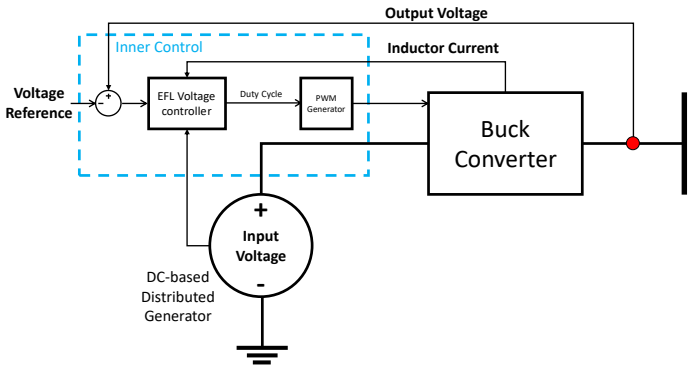

Figure 4.8: EFL voltage control schematic.

$$D(t) = \Bigg[- K_1 z_1(t) - K_2 z_2(t) + K_i e_i(t) + ... \\ ... \frac{1}{RC^2} x_1(t) + \left(\frac{1}{LC} - \frac{1}{(RC)^2} \right) x_2(t) \Bigg] \frac{LC}{E} \quad (4.31)$$

where $z_1 = e(t)$, is defined in function of the error, and z_2 is defined by the expression (4.25).

As explained in section 4.1.2, feedback of the input voltage E might ensure a fast response against changes in the DC bus. In voltage control (4.31) is dependant of the load resistance R. In a variable load node, R could change abruptly, leading to instabilities. In the buck converter case, this problem can be solved by doing a digital calculation of the resistances value, from the known values of i and v. With this feedback, the control law is strong enough to overcome several disturbances at the load side.

Fig. 4.7, shows a simplified schematic, in which the control law of (4.31) is embedded in the the inner control block.

4.2 Primary control:Droop control

The droop control is implemented as a primary control strategy in grid forming and grid supporting converters (see 3.1) in order to neglect the effects of the lines resistance among the DC-link circuit. Equation (4.32) shows the general form of the droop law, where V^{ref} is the reference voltage of the converter, V is the dc-link nominal voltage, R_d is the droop coefficient, and i_o is the source current.

$$V^{ref} = V + R_d i_o \quad (4.32)$$

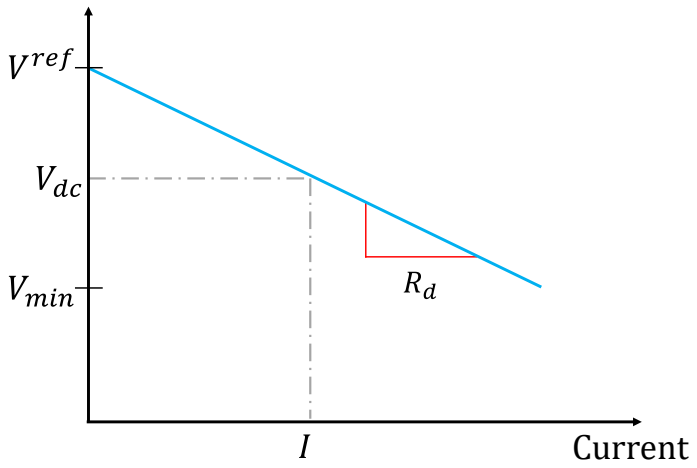

Figure 4.9: Voltage vs current graphic based on (4.32).

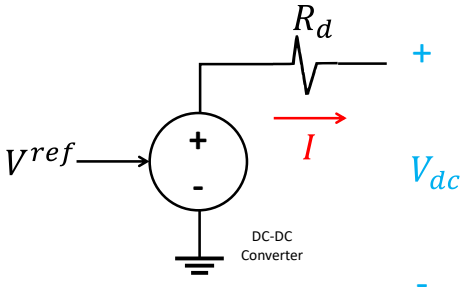

Figure 4.10: Simplified droop law circuit approach.

As can be seen, the droop law depicted in (4.32) has the general form of the line equation; this could be graphically represented in Fig 4.9, in which is easy to see that the droop gain is the slope of the line.

For that reason, R_d must be calculated such that it guarantees the stability of the system. Therefore the maximum allowable voltage variations, and the rated capacity of the converter are the factors that must be taken into account in the droop gain design procedure. This lead expression (4.33), where, I_n is the rated current of the converter, V_{min} is the minimum voltage deviation allowed, and V is the microgrid nominal voltage.

$$R_d = \frac{V - V_{min}}{I_n} \tag{4.33}$$

Otherwise R_d could be adjusted experimentally with a voltage regulation approach. The droop law (4.32) can be seen, electrically, as a voltage source (V^*) provided by the power electronic device, with (R_d) as a virtual series resistance as shown in Fig. 4.10. This simplified approach eases the simulation process.

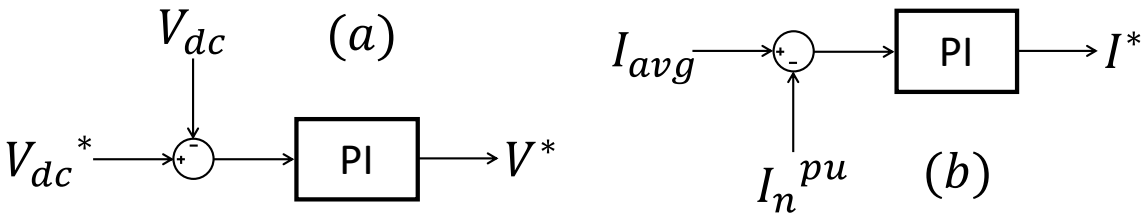

Figure 4.11: (a) Voltage regulator. (b) Current regulato.

Higher droop gains reduce the effect of line resistances on the current sharing accuracy, however, may cause large voltage drops in the output terminal of the converters [16].

Though The droop control acts as a primary proportional regulation that establish the output voltage reference of each converter in a microgrid, as every proportional control, has not reference tracking, so present a steady state error, known as voltage deviation. By itself, the droop law cannot guarantee the appropriate operation of the microgrid. To correct this issue a secondary control architecture must be implemented.

4.3 Secondary control

[16]

In chapter 2.3.3 a brief introduction to the main secondary control strategies was presented. In terms of reliability, efficiency and sturdiness, was said that the centralized architecture is the most accurate option in small microgrid applications.

4.3.1 DC link Voltage Regulation

Is expected that a centralized voltage regulator track a reference of the DC-link voltage, in a small microgrid, with a single DC-bus and relatively small line resistance, this task could be accomplished with a simple PI voltage controller as depicted in Fig. 4.11 (a). Where V_{dc}^* is the reference voltage of the DC-link, V_{dc} is the DC-link actual voltage, and V^* is the voltage reference of the distributed generators.

4.3.2 Current Regulation

Proportional power load sharing is a common term that refers a percentage sharing of the load, based on the nominal output values of each dispatchable DG unit. This is, that every DG contributes with the current injection according with its nominal capacity. A PI current control could achieve this goal as depicted in Fig. 4.11 (b).

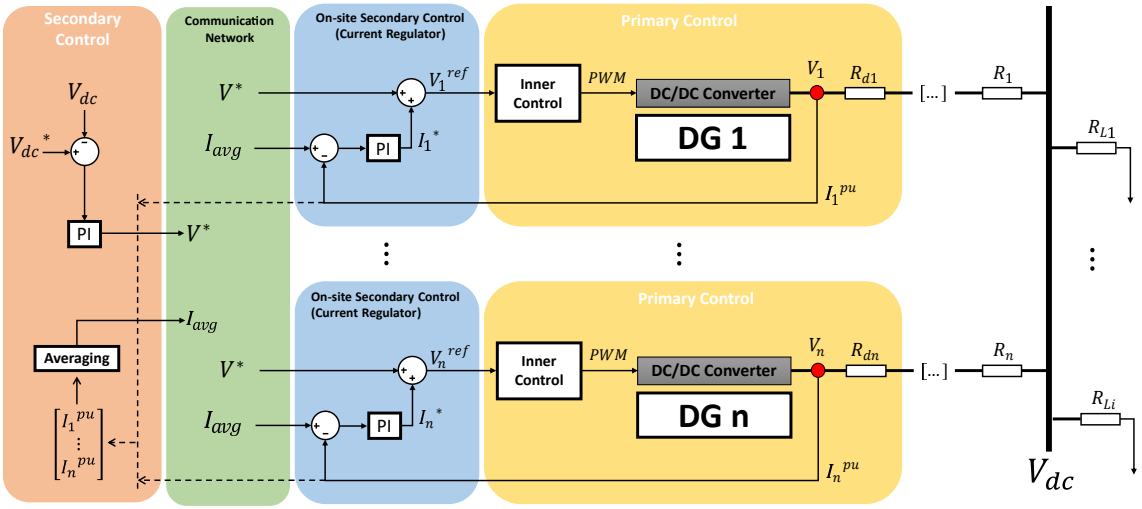

Figure 4.12: Diagram of a centralized control architecture with voltage and current regulation.

Where I_n^{pu} is the per-unit value of the current shared by the n DG, being n the number of dispatchable units, and I_{avg} is a value computed by the expression (4.34).

$$I_{avg} = mean\left([I_1^{pu}, ..., I_n^{pu}]^T\right) \tag{4.34}$$

This means that the current regulator has an on-site controller 4.11 (b), and a centralized estimator that computes the current reference I_{avg}

4.3.3 General scheme

.

The current regulator output I^* is added to the voltage regulator output V^* to compute the reference voltage of the droop law V^{ref}, and the per-unit value of the injected current I_n^{pu} is computed with (4.35), where I is the actual value of the injected current, and I_{nom} is the nominal current of the DG unit.

$$I_n^{pu} = \frac{I}{I_{nom}} \tag{4.35}$$

The hierarchical control scheme until the second layer could be summarized in Fig. 4.12, where $[R_1, ...Rn]$ are the line resistances, and $[R_{L1}, ...RLi]$ are the load resistances being i the number of loads.
To refer the control schematic that rules over the grid feeding converters see Fig. 4.7, the load side converters use the same structure than depicted by Fig. 4.8.

CHAPTER 5

Simulation Results

This chapter summarizes the results of the inner, primary and secondary control architectures developed in chapter 4 and tested with a simulation tool.

5.1 Feed back linearization control

5.1.1 Experimental Setup

Model constants

Table 5.1 shows the model parameters, taking into account the critical inductor and capacitor given by (4.3).

Gains of the PID are adjusted with the *PID tune* environment of Simulink® and are presented in the table 5.2.

The constants of the non-linear controllers K and K_i, for current control, and

Name	Symbol	Value
Input voltage	E	$220V$
Nominal output voltage	v_n	$24V$
Nominal inductor current	i_n	$16.66A$
Switching frequency	f	$80kHz$
Capacitance	C	$220\mu F$
Inductance	L	$6.7mH$
Resistance	R	1.44Ω
Equilibrium Duty Cycle	D^*	11%

Table 5.1: Simulation development.

PID CONTROLLER	Constant	Value
Current controller	K_i	106.830662
	K_p	0.106327
	K_d	$7.852402e-6$
Voltage controller	K_i	9.45698
	K_p	0.023592
	K_d	$1.15975e-5$

Table 5.2: Constants of the PID controllers.

EFL controller	Constant	Value
Current controller	K	$1.009e+04$
	K_i	$-9e5$
Voltage controller	K_1	$12.711e6$
	K_2	15.845
	K_i	$-54e7$

Table 5.3: EFL control Constants.

K_1, K_2 and K_i, for voltage control, are adjusted experimentally and are shown in table 5.3.

Simulation Settings

Simulations are made in Matlab-Simulink® with a duration of $230ms$. All controllers begin with the reference value in 0 and have a reference change at $t = 5ms$. For current control, the new reference is set to i_n, and for voltage control, the reference is set to v_n. In order to test the controllers' robustness, two different disturbances are programmed, the first one at $t = 110ms$, an input voltage loss of 30%. The second one, at $t = 150ms$, is a parallel connection of a resistive load equal to R's nominal value, simulating a sudden load increase.

To compare the performance of the EFL and PID controllers, mean square error (MSE) and Integral time absolute error (ITAE) are applied to each simulation and compared in tables 5.4 and 5.5.

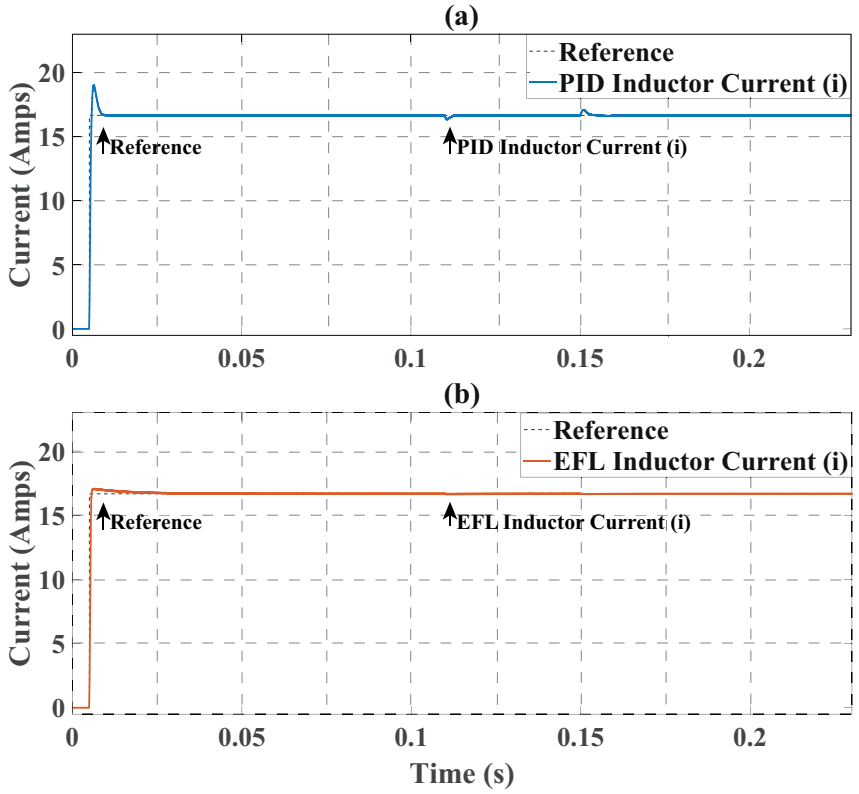

Figure 5.1: Current control performance: (a) PID. (b) EFL.

5.1.2 Results and discussion

Current control

In Fig. 5.1 is depicted the response of PID (a) current controller, and EFL (b) current controller whose control law is defined by the expression (4.23). Note that both methods fulfill the objective, reaching the reference and overcoming the disturbances.

Due to the speed of both responses, a detailed analysis is presented. In Fig. 5.2 is shown the transitory response to the reference change at $t = 5ms$. There is a clear difference between both graphs. Fig. 5.2 (a), depicts a maximum overshoot of $2.3649A$ and a settling time less than $5ms$, instead Fig. 5.2 (b), depicts a maximum overshoot of $0.3963A$ and a settling time of $20ms$. It can be concluded that the EFL, although it is slower than the PID, has a better transient response.

Fig. 5.3 depicts a zoom over the disturbances between $t = 100ms$ and $t = 200ms$. Note that PID (a), has a current loss of $0.3347A$ at $t = 110ms$ due to the first disturbance. The same graph depicts a current increment of $0.4371A$ at $t = 150ms$ due to the load connection. EFL (b) does not present representative changes against any of the disturbances, showing more sturdiness than the PID control.

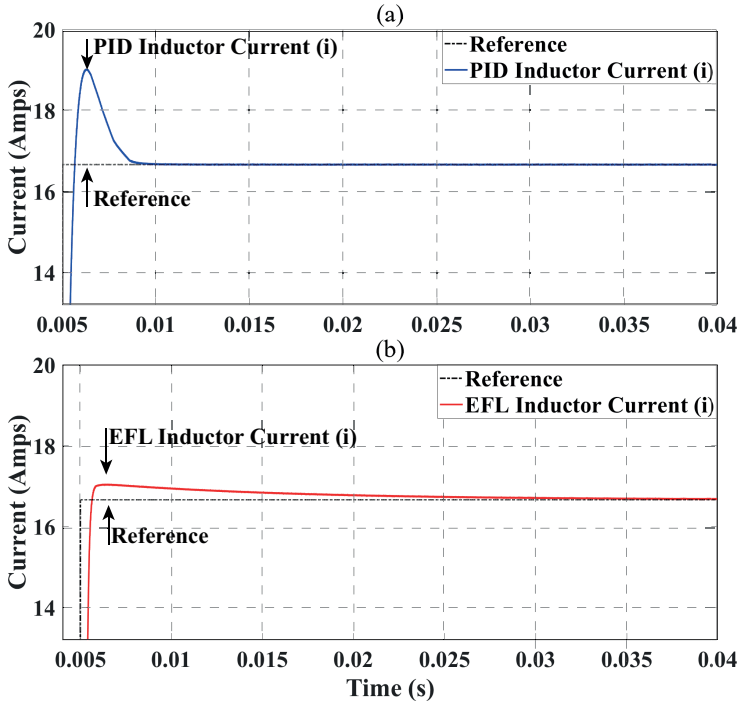

Figure 5.2: Current control transient state behaviour: (a) PID. (b) EFL.

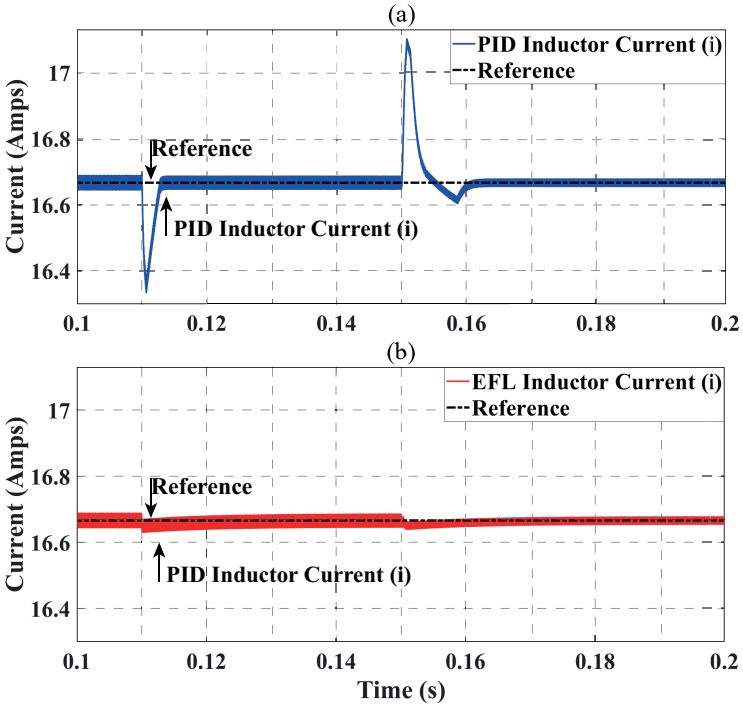

Figure 5.3: Current control disturbance response behaviour: (a) PID. (b) EFL .

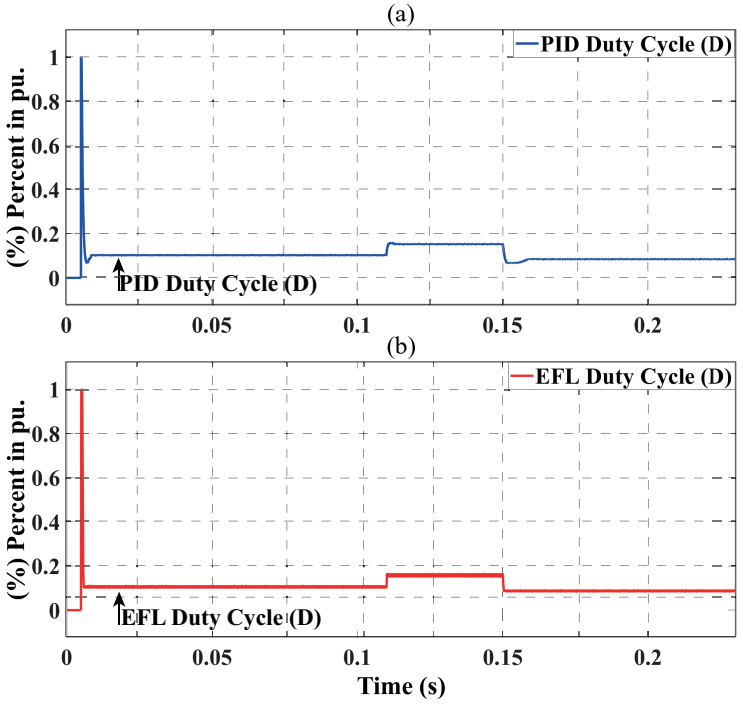

Figure 5.4: Current control duty cycle comparison: (a) PID. (b) EFL.

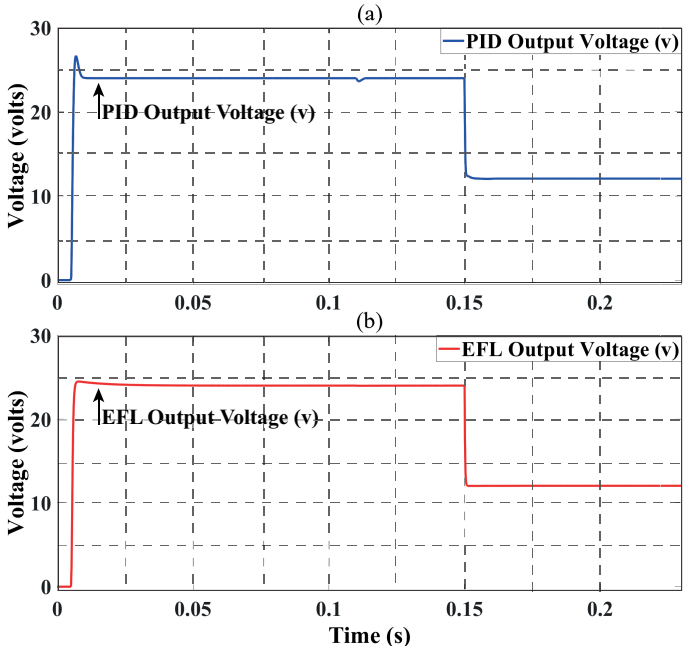

Figure 5.5: Current control voltage response comparison: (a) PID. (b) EFL.

Control method	**MSE**	**ITAE**
PID	$2.6482e+05$	$2.1765e+03$
EFL	$2.3316e+05$	$1.5045e+03$

Table 5.4: Comparison of current controllers performance.

Fig. 5.4 shows the performance of the control signal, the duty cycle (D), through all the simulation. It can be seen that PID response (a), and EFL response (b), have a similar behaviour, with a slightly difference at the disturbances response, at $t = 5ms, 110ms, 150ms$. It is worth noting that the PID is slower but has less oscillations, meanwhile the EFL is faster, and virtually avoids the overshoots caused by the disturbances. The output voltage response (v) presented in Fig. 5.5 shows the voltage behaviour through all the simulation, showing a sudden voltage loss at $t = 150ms$ due to the second load connection, equivalent to a half o the nominal output voltage $v = 12V$. To clarify the results, table 5.4 compare the MSE and ITAE measures of both controllers, where the higher performance of the current EFL controller is validated.

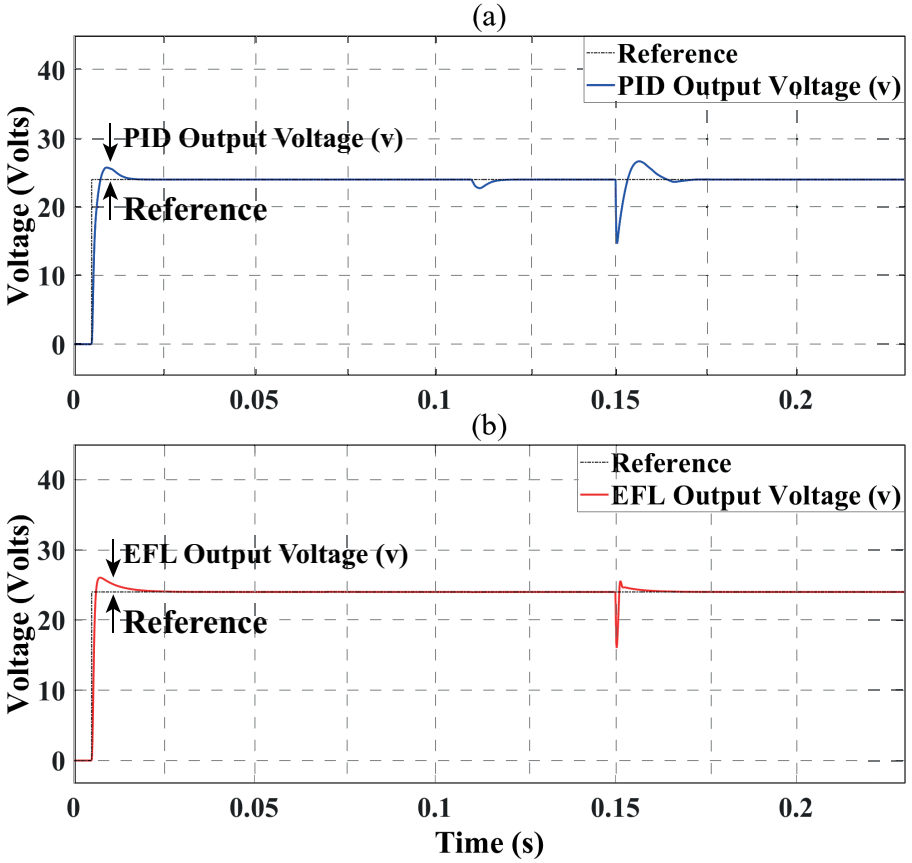

Figure 5.6: Voltage control performance: (a) PID, (b) EFL.

Voltage control

Fig. 5.6 is depicts the response of PID (a), and EFL (b) whose control law is defined by expression (4.31).

Transient response is clearer presented in Fig. 5.7, where PID (a), have a maximum overshoot of $1.7545V$, and a settling time less than $15ms$. In contrast, EFL (b), have a maximum overshoot of $2.0498V$, and a settling time less than $26ms$. In this case, PID control shows a better transient response. Disturbances response is depicted in Fig. 5.8. The input voltage loss at $t = 110ms$, in PID graph (a), induce a sudden oscillation with a negative peak of $1.2738V$. Note that this disturbance is virtually ignored by the EFL (b). It can be seen that the extra load connection at $t = 150ms$ trigger a highly oscillatory response in both methods. On the other hand, the PID reaches a maximum deviation of $9.3431V$. However, the EFL reaches a maximum deviation of $7.9628V$. Therefore, the EFL with input voltage (E), and load (R) feedback, demonstrate better sturdiness than the PID control.

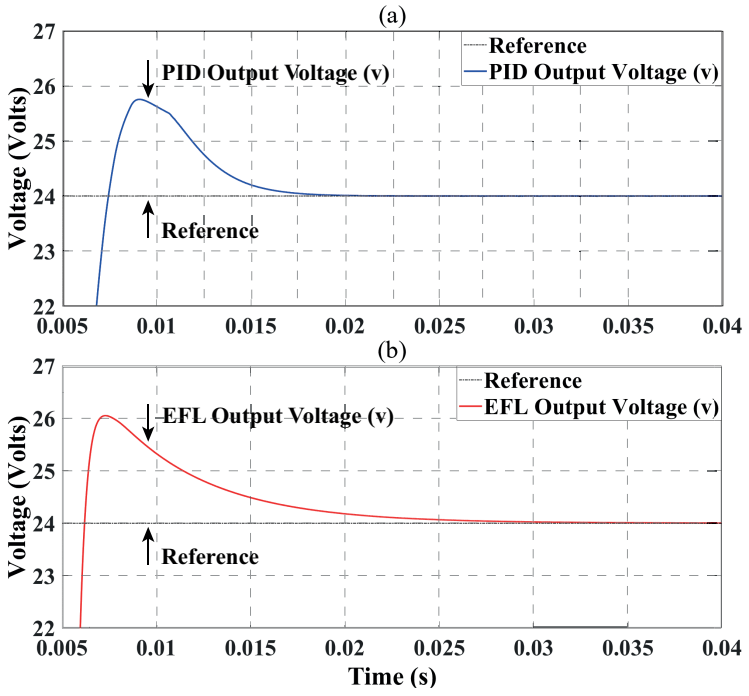

Figure 5.7: Voltage control transient response behaviour: (a) PID. (b) EFL.

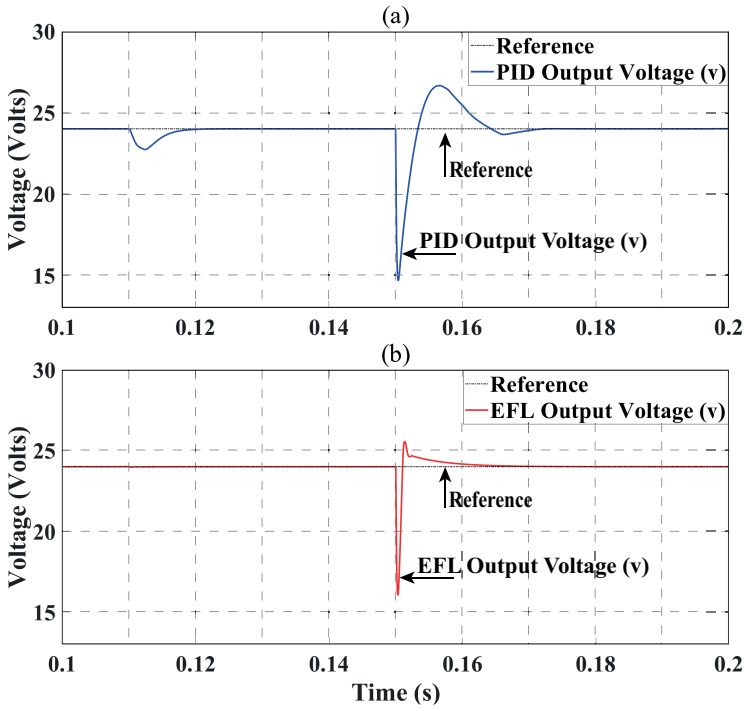

Figure 5.8: Voltage control disturbance response comparison: (a) PID. (b) EFL.

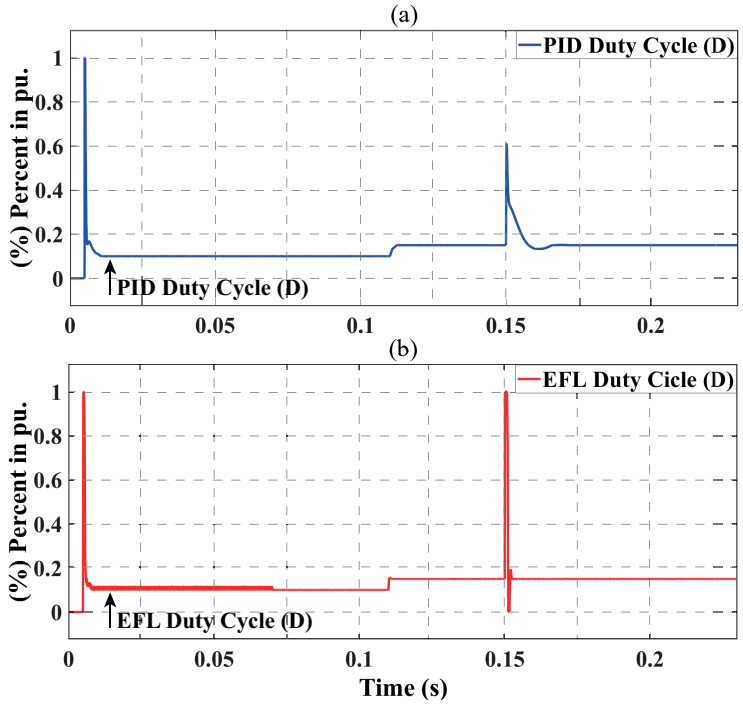

Figure 5.9: Voltage control, duty cycle comparison: (a) PID. (b) EFL.

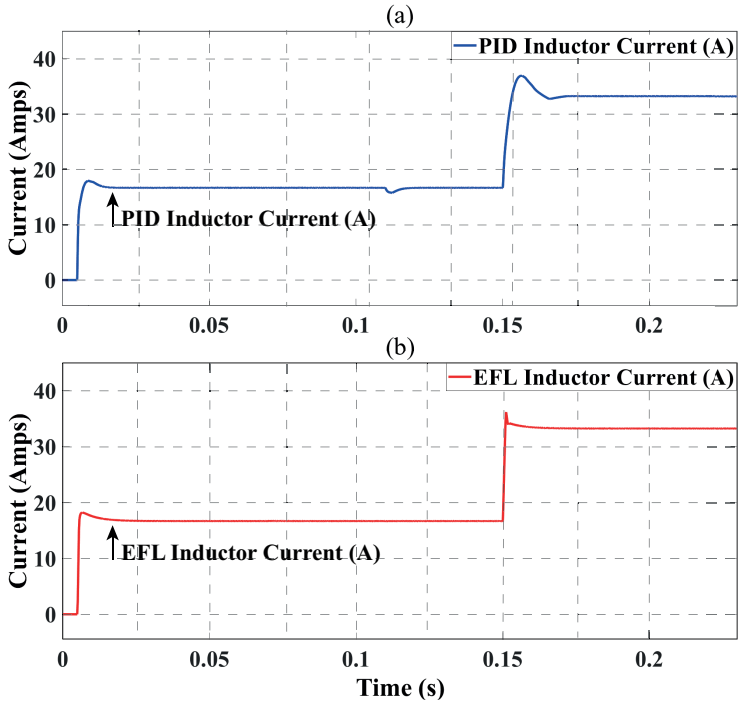

Figure 5.10: Voltage control, inductor current response: (a) PID. (b) EFL.

The control signal comparison is presented in Fig. 5.9. In this case EFL (b), have a more aggressive response compared with the PID (a). In order of overcome the disturbances at $t = 150ms$, the EFL duty cycle shows a higher oscillatory peak.

Behaviour of the current with the voltage controllers is presented in Fig. 5.10. It can be seen that both models ensure acceptable stability even in front of major disturbances. At $t = 150ms$ the second load is connected in parallel, demanding an increase on the output current, equivalent to the nominal value of the inductor current $i = 16.66A$. To clarify the results, table 5.5 compare the MSE and ITAE measures resulting from the experimental setup for both controllers. In this case, the higher performance of the voltage EFL controller against the voltage PID controller, is proved by a narrow margin.

Control method	**MSE**	**ITAE**
PID	$2.0264e+06$	$2.8987e+04$
EFL	$1.3401e+06$	$8.8262e+03$

Table 5.5: Comparison of voltage controllers performance.

These experimental results are summarized in Ref. [36].

5.2 Simulation of the microgrid

5.2.1 Experimental Setup

Fig. 5.11 show the general structure of the microgrid tested in the simulation tool. Three different DGs with different line resistances are connected to a common DC-bus. The DGs configuration obeys all the theory documented in chapters 3,4. Note the switches S_1, S_2 are included to simulate two different disturbances. All the variables involved in the microgrid control are average values, this due to the converters commutation, that cause interruptions in the current flux.

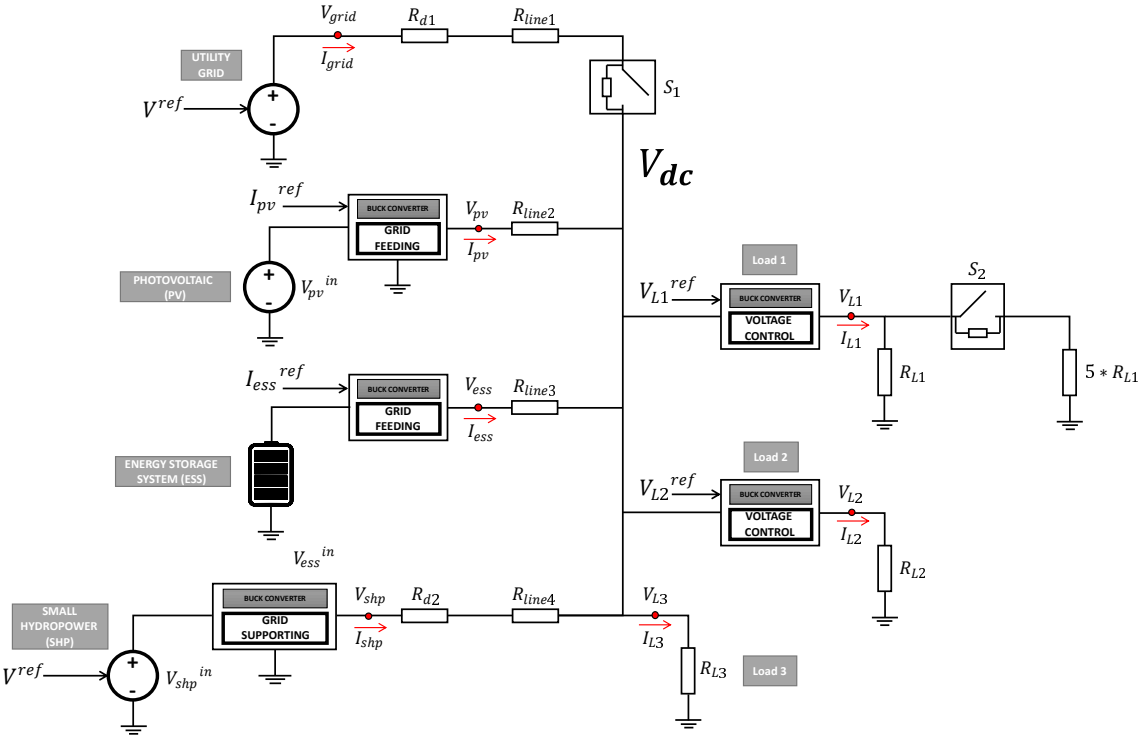

Figure 5.11: Experimental setup of the microgrid.

Model constants

Internal constant parameters of the converters, inductance and capacitance, are the same of the table 5.1. In order to test the EFL method in different conditions, some variations were considered in each of the converters and the whole microgrid operation.
Table 5.6 refers the properties of the grid forming/supporting nodes which inner control strategy is the voltage controller described in the section 4.1.2.

Forming/Supporting node	Name	Value
Utility grid (Forming)	Input voltage (Controlled variable)	-
	Nominal output voltage	$380V$
	Nominal inductor current (controlled variable)	$30A$
	Line resistance	0.01Ω
	Drop coefficient R_d	0.09
SHP (Supporting)	Input voltage (controlled variable)	$1200V$ (Nominal)
	Nominal output voltage	$380V$
	Nominal inductor current (controlled variable)	$25A$
	Line resistance	0.204Ω
	Drop coefficient R_d	0.1

Table 5.6: Grid forming/supporting Nodes nominal parameters.

DG node	Name	Value
PV	Input voltage	$760V$
	Output voltage	$380V$
	Nominal inductor current (controlled variable)	$20A$
	Line resistance	0.4Ω
ESS	Input voltage	$645V$
	Output voltage	$380V$
	Nominal inductor current (controlled variable)	$15A$
	Line resistance	0.2Ω

Table 5.7: Grid feeding node's nominal parameters.

Load converters nominal parameters	Name	Value
Load 1	Input voltage	$380V$
	Output voltage (controlled variable)	$48V$
	Nominal inductor current	$41.66A$
	Nominal resistance (R_{L1})	1.1520Ω
Load 2	Input voltage	$380V$
	Output voltage (controlled variable)	$36V$
	Nominal inductor current	$31.25A$
	Nominal resistance (R_{L2})	1.1520Ω
Load 3 (Directly connected to the DC-link)	Input voltage	$380V$
	Nominal resistance (R_{L3})	7Ω

Table 5.8: DC/DC load interfaces nominal parameters.

Table 5.7 refers the parameters of the grid supporting nodes that have integrated the current controllers developed in the section 4.1.2 and which results are presented in section 5.1.2. The nominal inductor current parameter is used as current references in order to simulate the MPPT operation.

The parameters of the load-side converters are depicted in table 5.8. L_1 converter isolates a $48V$ DC-link, and L_2 isolates a $36V$ DC-link.These devises imitate a microgrid with different voltage levels. In order of simplify the simulation, the

considered AC loads were changed for L_3, note that this node is directly connected to the DC Voltage line, and has a relative low resistance value.

The constants of the EFL have to be adjusted in each new application of the buck converters. The new gains are depicted in table 5.9. Each case required an experimental adjustment.

Converter Node	**Constant**	**Value**
PV, ESS	K	6060
	K_i	$-3.6e5$
SHP	K_1	$1.36e5$
	K_2	820
	K_i	$-2.4e6$
Loads 1, 2	K_1	$12.474e6$
	K_2	$15.83e3$
	K_i	$-36e7$

Table 5.9: EFL control constants.

The PI constants of the voltage and current regulator are shown in table 5.10. The tuning of this gains was made through experimental analysis.

PI controller	**Constant**	**Value**
Current regulator	K_i	1600
	K_p	800
Voltage regulator	K_i	200
	K_p	0.5

Table 5.10: PI control regulators constants.

Simulation Settings

The simulation was made in Matlab-Simulink® with a duration of $800ms$. All control references begin with their nominal values. Grid forming/supporting node's output voltage, is controlled by the voltage and current regulator as depicted in Fig. 4.12 and Fig. 5.11, whose references are the DC-link nominal voltage ($380V$) and the estimated average current (I_{avg}).

In order to test the controllers' robustness, two different disturbances were programmed in the switch's S_1 and S_2. The first one at $t = 250ms$, S_2 normally open, is closed, inducing a parallel connection of a resistive load equal to $5R_{L1}$, simulating a sudden load increase in L_1 node. The second one, the disconnection of the utility grid at $310ms$, when normally closed S_1 is opened, simulating a forced isolating of the microgrid, testing the capacity of the SHP node of maintaining the DC-link voltage, and all interfaces sturdiness.

5.2.2 Results and discussions

Below are presented the results of the microgrid simulation.

Fig. 5.12, show the current behaviour of all the DG units. (a) Is the response through all the simulation. (b) Is a zoom of the transient response in which is evident a high overshoot of the grid current of $16.223A$ around 100% of the steady state value, is evident that all the DG units have a better behaviour. The overall settling time is approximately $20ms$. (c) Is a zoom of the response against the first perturbation, a medium overshot of $6.761A$ is visible among all the DGs. The settling time is around $15ms$, is visible too, how the dispatchable units work together in order to supply the extra load current requirement. (d) Is the zoom of the isolation behaviour, at $t = 310ms$ the utility grid is disconnected through the opening of S_1, the new grid forming node is now the SHP generator, is easy to see how the current injection of this node grows in proportion to the supply loss of the utility grid. The overshoot for SHP is $2.8633A$, around 9.87% of the steady state value and, the grid feeding sources experiment a perturbation of $6A$ for PV node and $7A$ for ESS node. The whole isolation process has a settling time of $328ms$.

Fig. 5.13 show the behaviour of the DGs output voltage. (a) Is the whole simulation graphic. (b) Is the transient state response zoom, showing a smooth transition whit a negligible overshoot of $6.19V$ around 1.63% of the steady state value and a estimated settling time of $50ms$. (b) Shows the response against the first disturbance, with an average voltage loss of $13.07V$ around the 3.5% of the steady state value, and a settling time of $26.9ms$. Finally, a considerable oscillation is triggered by the utility grid disconnection, the voltage loss reach $85.06V$ a 23% of the steady state value, but the disturbances is controlled in approximately $190ms$.

Fig. 5.14 compares the performance of the DC-link voltage against its reference. Note that the signal follows the behaviour of the voltages in Fig. 5.13, but tracking the nominal voltage reference.

Plot. 5.15 shows the performance of the internal current of the DG's converters. The grid feeding nodes response are compared whit the respective reference value, is clear that this nodes exceeds in the current control performance. The case of the SHP source is not less important, a fast response against perturbations ensures the stability of the microgrid, even without the utility grid support.

Other information about the controllers response is available on Fig. 5.16. The performance of the internal control signal (duty cycle) shows smooth changes against the disturbances and no saturation even in the isolation process.

The analysis of the responses at the loads-side of the microgrid must be done. A interesting behaviour is depicted in Fig. 5.17, that shows the current consumption at the load converters input. When this graph is compared with Fig. 5.12 (a), is possible to check that the addition of all the DG's current injection is equal to the addition of all the load input current consumption. Is important to note

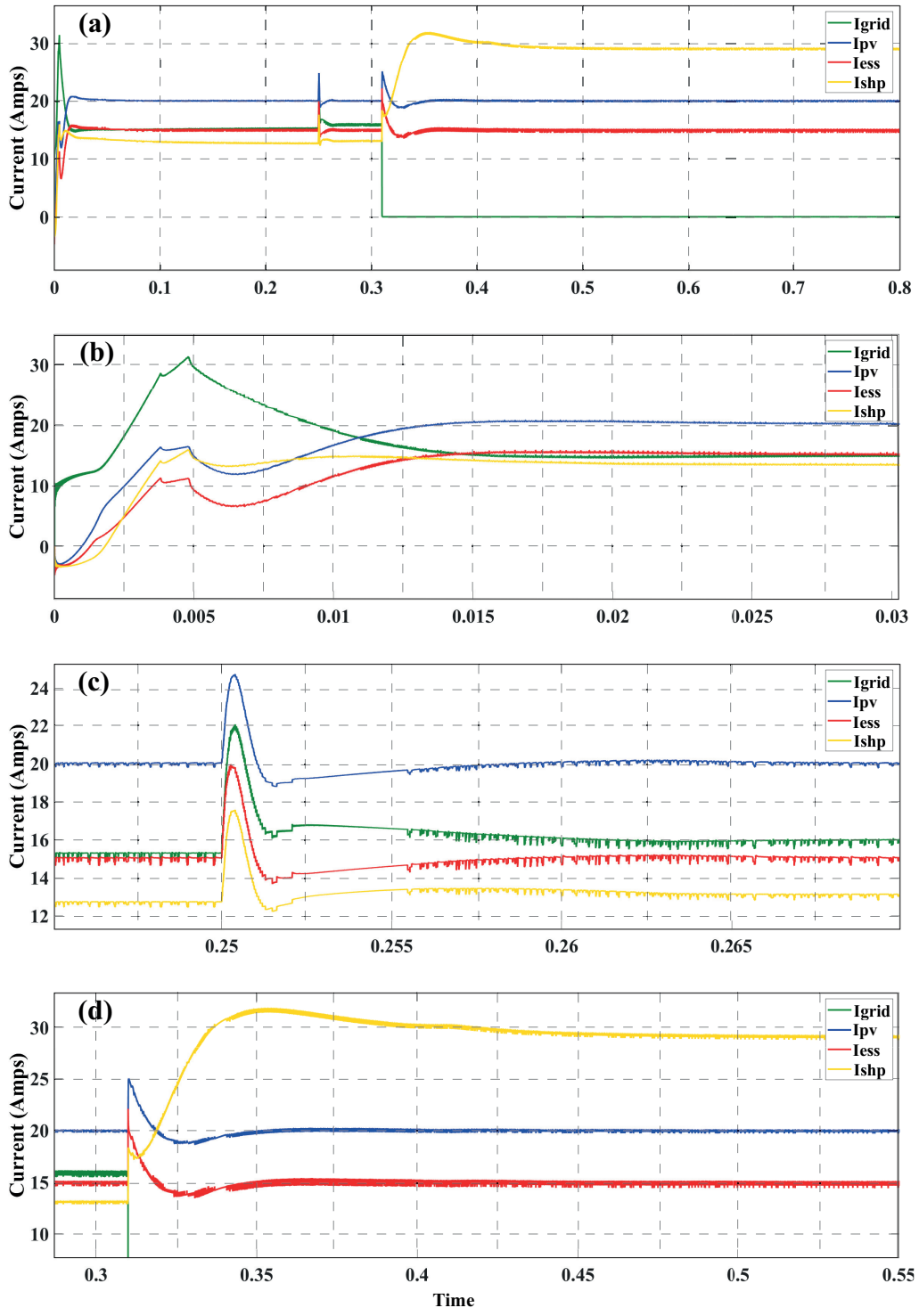

Figure 5.12: (a) DGs current injection response. (b) Transient state response. (c) Load connection response. (d) Grid islanded operation mode.

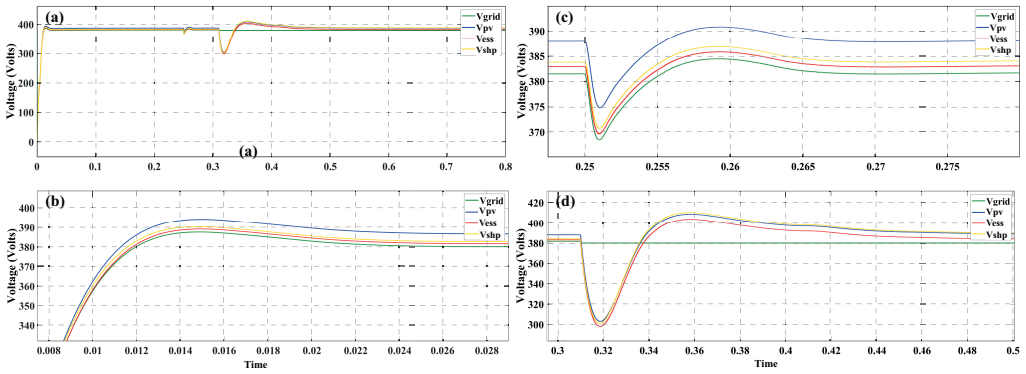

Figure 5.13: (a) DGs voltage output. (b) Transient state response. (c) Load connection response. (d) Grid islanded operation mode.

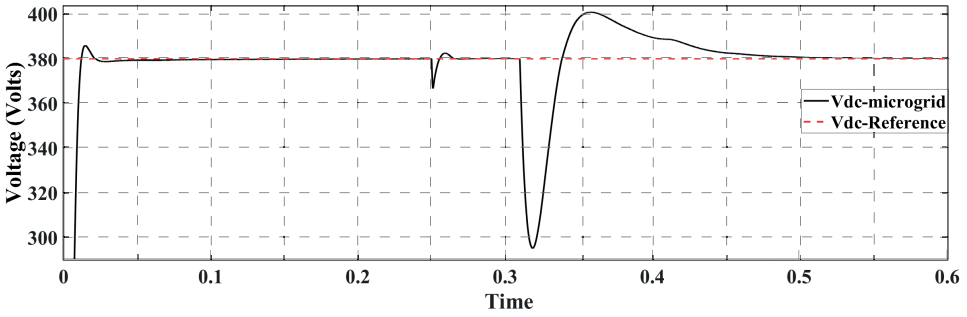

Figure 5.14: DC-Link voltage behaviour.

the disturbances effects among the graphs. The addition of extra load in L_1 at $t = 250ms$ causes a sudden current increase in I_{L1}, but this doesn't affect drastically the behaviour of the rest of load nodes. Instead, the disconnection of the microgrid at $t = 310ms$ visibly affects L_3, since this load is directly connected to the DC-link, the current is dependent of its variations. Remarkable conclusions can be drawn from this result.

Finally, in order to check the controllers sturdiness, Fig. 5.18 (a) shows the response of the currents at the output of the DC/DC interfaces, is clear that the firs disturbance increases the current consumption in a 20% of the original value for L_1 node; out of that, any disturbance is visible through all the simulation time. Plot (b) shows the output voltage of the load DC/DC interfaces compared with the references values, the first disturbance triggers a small voltage loss that is quickly corrected.

Fig. 5.19 present the behaviour of the duty cycle of the load interfaces. The ability of read the input voltage changes, clearly improve the performance of the EFL inner controllers.

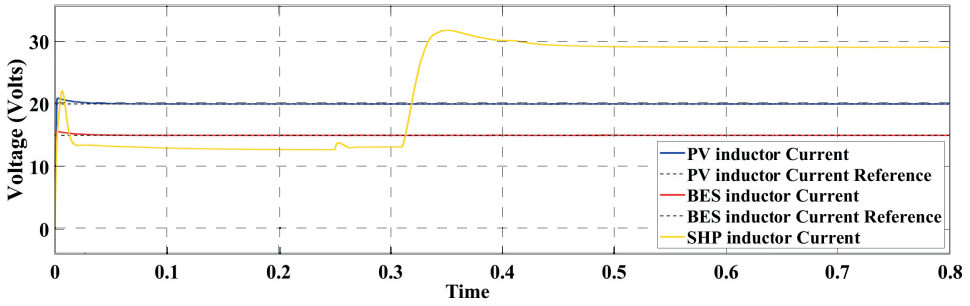

Figure 5.15: Distributed generators inductor currents response.

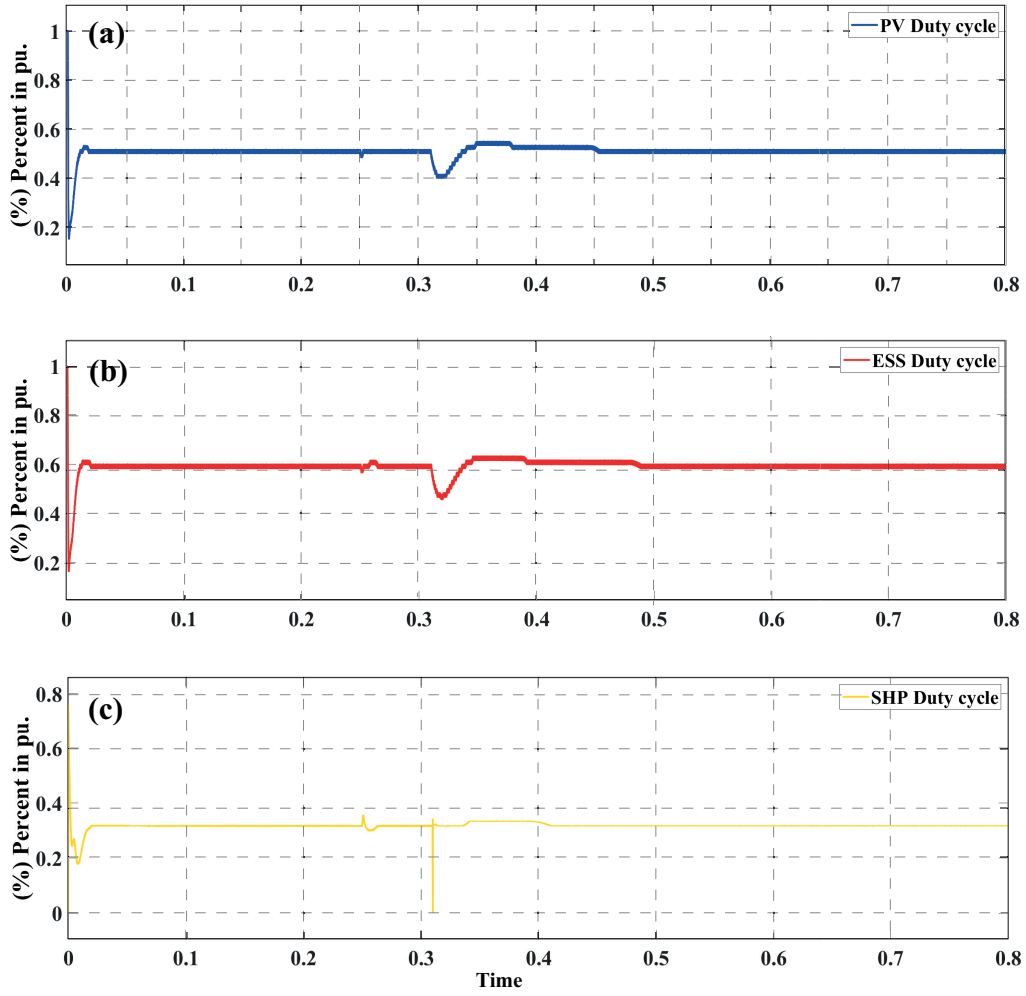

Figure 5.16: Duty cycle of the distributed generators response. (a) PV node. (b) ESS node. (c) SHP power node.

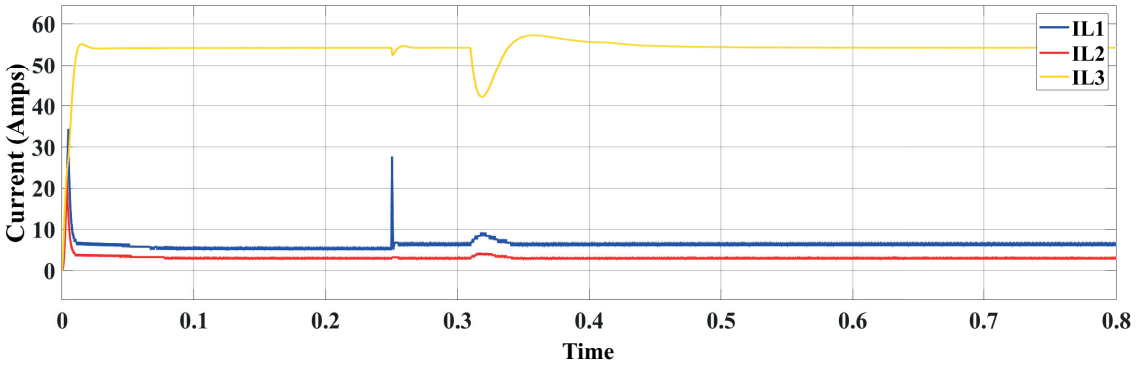

Figure 5.17: Loads input current.

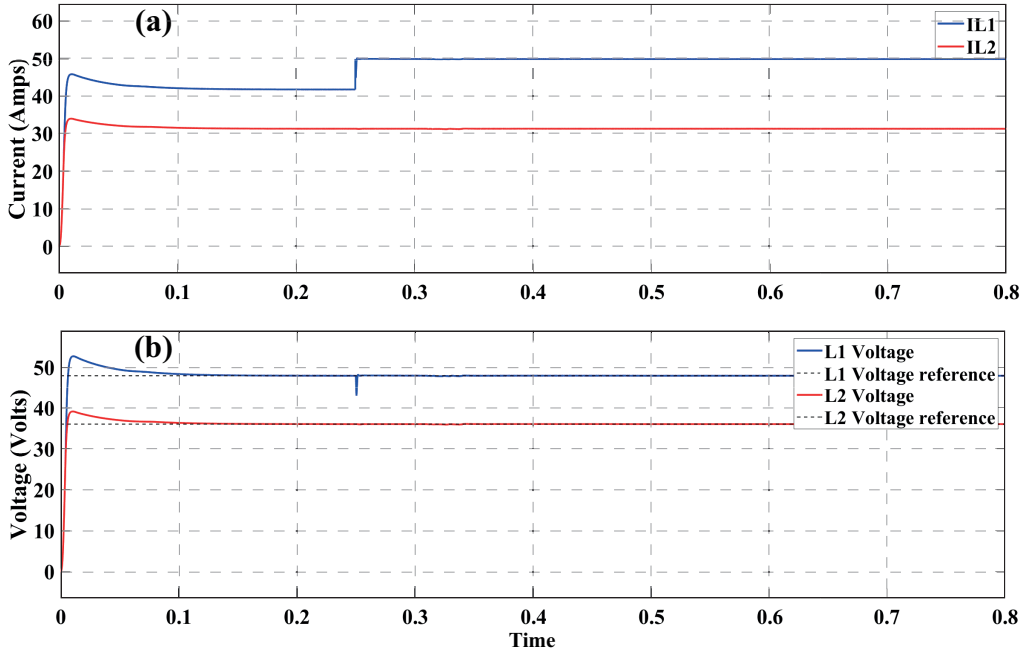

Figure 5.18: (a) Current consumption of isolated loads. (b) DC/DC interfaces output voltages.

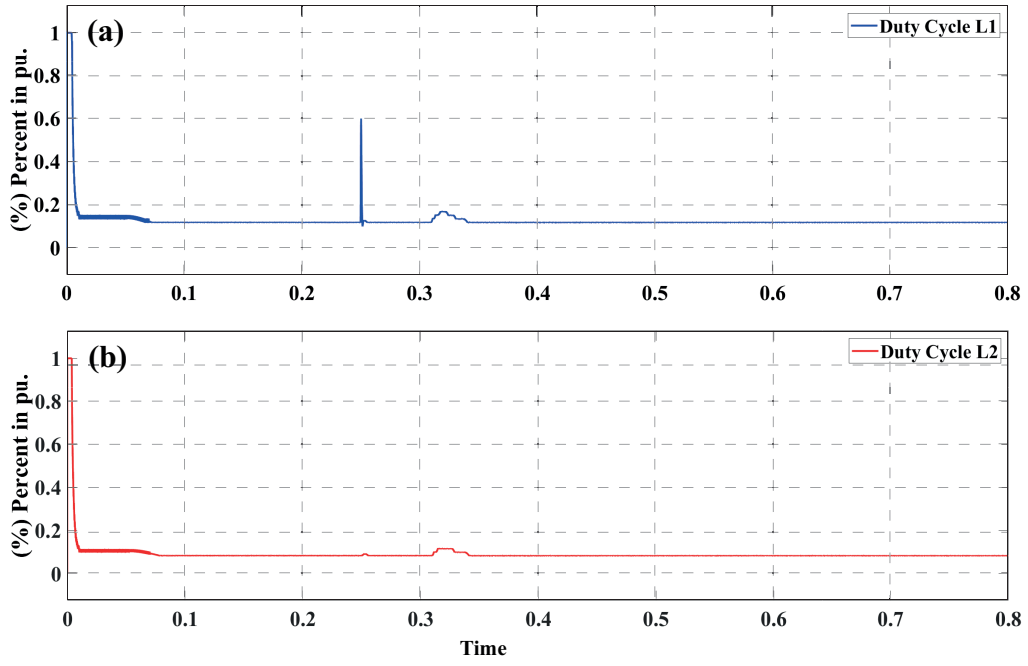

Figure 5.19: Duty Cycle of the load DC/DC interfaces. (a) Load 1. (b) Load 2.

CHAPTER 6

Conclusions

The first chapters of this project highlight the importance of the investigation in the field of renewable energy's and the open issues that have to deal with. Summarized research about the microgrids history, characteristics, and architectures was done. The relevance of appropriating these topics as a society, motivates the design of a low scale microgrid, thought for the countryside, with the purpose of take advantage of the almost, inexhaustible distributed energy resources that Colombia has.

In the theoretical frame, to validate the feedback linearization control theory, two different internal EFL controllers for current and voltage regulation of a Buck converter were designed, tested, and compared to a well-known PID control method. Despite being based in a reduced order model, the current controller shows better performance and sturdiness than the usual PID. Another feature of this controller is its simplicity and relative easy adjustment. The non-linear voltage controller has shown a slight advantage compared to the PID, but, just like the PID, the difficulty to tune the controller parameters adequately adds complexity to the tuning. However, these controllers have proved sturdiness and reliability under complex simulation arrangements. The microgrid operation shows a stable behaviour and smooth transitions against the tested disturbances, especially in the forced isolation event, that is considered a basis of the microgrid operation.

More research is needed to reach a better understanding of microgrids control architecture and design. The comparison between different schemes (centralized, decentralized, distributed) to reach the ideal one, the implementation of disconnection and connection protocols, the addition of the third control layer that search for regulating the economic dispatch, the research about better management of the energy storage systems, and the junction of AC and DC technologies in hybrid microgrids, are relevant investigation axes in this topic.

Bibliography

[1] S. Parhizi, H. Lotfi, A. Khodaei, and S. Bahramirad, "State of the art in research on microgrids: A review," *IEEE Access*, vol. 3, pp. 890–925, 2015.

[2] R. H. Lassater, "MicroGrids," in *2002 IEEE Power Engineering Society Winter Meeting. Conference Proceedings (Cat. No.02CH37309)*. New York, NY, USA, USA: IEEE, 2002, pp. 305–308. [Online]. Available: https://ieeexplore.ieee.org/abstract/document/985003

[3] L. Fusheng, L. Ruisheng, and Z. Fengquan, *Microgrid Technology and Engineering Application*. Joe Hayton, 2016. [Online]. Available: http://www.sciencedirect.com/science/article/pii/B9780128035986000115

[4] P. Brian, "DC, Come Home: DC Microgrids and the Birth of the "Enernet"," *IEEE Power and Energy Magazine*, vol. 10, no. 6, pp. 60–69, 2012.

[5] H. García, A. Corredor, L. Calderón, and M. Gómez, "Análisis Costo Beneficio De Energías Renovables No Convencionales En Colombia," *Fedesarrollo - Documento preparado para WWF*, p. 90, 2013. [Online]. Available: http://www.fedesarrollo.org.co/wp-content/uploads/2011/08/WWF_Analisis-costo-beneficio-energias-renovables-no-convencionales-en-Colombia.pdf

[6] D. C. Mora Navarro and J. M. Hurtado Liévano, "Guía para el estudio de prefactibilidad de pequeñas centrales hidroeléctricas como parte de sistemas híbirdos." Ph.D. dissertation, Pontificil Universidad Javeriana, 2004.

[7] E. Planas, J. Andreu, J. I. Gárate, I. Martínez De Alegría, and E. Ibarra, "AC and DC technology in microgrids: A review," 2015.

[8] J. J. Justo, F. Mwasilu, J. Lee, and J. W. Jung, "AC-microgrids versus DC-microgrids with distributed energy resources: A review," *Renewable and Sustainable Energy Reviews*, vol. 24, pp. 387–405, 2013. [Online]. Available: http://dx.doi.org/10.1016/j.rser.2013.03.067

[9] M. F. Akorede, H. Hizam, and E. Pouresmaeil, "Distributed energy resources and benefits to the environment," *Renewable and Sustainable Energy Reviews*, vol. 14, no. 2, pp. 724–734, 2010.

[10] B. Hernandez, E. Giraldo, S. Ospina, and A. Garces, "Master-slave operation of DC microgrids: An adaptive control approach with estimation," in *4th IEEE Colombian Conference on Automatic Control: Automatic Control as Key Support of Industrial Productivity, CCAC 2019 - Proceedings*, 2019.

[11] M. S. Mahmoud and N. M. Alyazidi, "Pilot-Scale Implementation of Coordinated Control for Autonomous Microgrids," pp. 341–367, 2016.

[12] Y. Han, W. Chen, and Q. Li, "Modeling, control, and energy management for DC microgrid," *Smart Power Distribution Systems*, pp. 69–90, 2019. [Online]. Available: https://linkinghub.elsevier.com/retrieve/pii/B9780128121542000043

[13] J. Kumar, A. Agarwal, and V. Agarwal, "A review on overall control of DC microgrids," *Journal of Energy Storage*, vol. 21, no. November 2018, pp. 113–138, 2019. [Online]. Available: https://doi.org/10.1016/j.est.2018.11.013

[14] A. Mehrizi-Sani, "Distributed Control Techniques in Microgrids," *Microgrid: Advanced Control Methods and Renewable Energy System Integration*, pp. 43–62, 2016.

[15] H. Yang, Q. Li, and W. Chen, "Microgrid communication system and its application in hierarchical control," *Smart Power Distribution Systems: Control, Communication, and Optimization*, pp. 179–204, 2018.

[16] S. Peyghami, H. Mokhtari, and F. Blaabjerg, *Hierarchical Power Sharing Control in DC Microgrids*. Elsevier Inc., 2016. [Online]. Available: http://dx.doi.org/10.1016/B978-0-08-101753-1.00003-6

[17] Y. Khayat, J. M. Guerrero, H. Bevrani, Q. Shafiee, R. Heydari, M. Naderi, T. Dragicevic, J. W. Simpson-Porco, F. Dorfler, M. Fathi, and F. Blaabjerg, "On the Secondary Control Architectures of AC Microgrids: An Overview," *IEEE Transactions on Power Electronics*, vol. 35, no. 6, pp. 6482–6500, 2020.

[18] B. Wunder, L. Ott, J. Kaiser, Y. Han, F. Fersterra, and M. Marz, "Overview of different topologies and control strategies for DC micro grids," *2015 IEEE 1st International Conference on Direct Current Microgrids, ICDCM 2015*, pp. 349–354, 2015.

[19] M. Shahbazi and A. Khorsandi, *Power Electronic Converters in Microgrid Applications*. Elsevier Inc., 2016. [Online]. Available: http://dx.doi.org/10.1016/B978-0-08-101753-1.00010-3

[20] A. G. Tsikalakis and N. D. Hatziargyriou, "Centralized control for optimizing microgrids operation," *IEEE Power and Energy Society General Meeting*, pp. 1–8, 2011.

[21] G. Agundis-Tinajero, N. L. D. Aldana, A. C. Luna, J. Segundo-Ramirez, N. Visairo-Cruz, J. M. Guerrero, and J. C. Vazquez, "Extended-Optimal-Power-Flow-Based Hierarchical Control for Islanded AC Microgrids," *IEEE Transactions on Power Electronics*, vol. 34, no. 1, pp. 840–848, 2019.

[22] N. L. Díaz, A. C. Luna, J. C. Vasquez, and J. M. Guerrero, "Centralized Control Architecture for Coordination of Distributed Renewable Generation and Energy Storage in Islanded AC Microgrids," *IEEE Transactions on Power Electronics*, vol. 32, no. 7, pp. 5202–5213, 2017.

[23] A. Bani-Ahmed, M. Rashidi, A. Nasiri, and H. Hosseini, "Reliability Analysis of a Decentralized Microgrid Control Architecture," *IEEE Transactions on Smart Grid*, vol. 10, no. 4, pp. 3910–3918, 2019.

[24] Q. Shafiee, V. Nasirian, J. M. Guerrero, F. L. Lewis, and A. Davoudi, "Team-oriented adaptive droop control for autonomous AC microgrids," *IECON Proceedings (Industrial Electronics Conference)*, pp. 1861–1867, 2014.

[25] M. Cucuzzella, G. P. Incremona, and A. Ferrara, "Decentralized Sliding Mode Control of Islanded AC Microgrids With Arbitrary Topology," *IEEE Transactions on Industrial Electronics*, vol. 64, no. 8, pp. 6706–6713, 2017.

[26] Y. Hakuto, T. Tsuji, and J. Qi, "Autonomous decentralized stabilizing control of DC microgrid," *2017 IEEE 2nd International Conference on Direct Current Microgrids, ICDCM 2017*, pp. 292–296, 2017.

[27] S. Anand, B. G. Fernandes, and J. M. Guerrero, "Distributed control to ensure proportional load sharing and improve voltage regulation in low-voltage DC microgrids," *IEEE Transactions on Power Electronics*, vol. 28, no. 4, pp. 1900–1913, 2013.

[28] Y. Shan, J. Hu, Z. Li, and J. M. Guerrero, "A Model Predictive Control for Renewable Energy Based AC Microgrids Without Any PID Regulators," *IEEE Transactions on Power Electronics*, vol. 33, no. 11, pp. 9122–9126, 2018.

[29] J. Lai, X. Lu, F. Wang, P. Dehghanian, and R. Tang, "Broadcast gossip algorithms for distributed peer-to-peer control in AC microgrids," *IEEE Transactions on Industry Applications*, vol. 55, no. 3, pp. 2241–2251, 2019.

[30] X. Li, Q. Xu, and F. Blaabjerg, "Adaptive Resilient Secondary Control for Islanded AC Microgrids With Sensor Faults," *IEEE Journal of Emerging and Selected Topics in Power Electronics*, vol. 6777, no. c, pp. 1–1, 2020.

[31] S. O. Hurtado, *ANÁLISIS DE CONTROLADORES NO LINEALES PARA CONVERTIDOR DC-DC TIPO BUCK-BOOST APLICADO A UN GENERADOR EÓLICO*. Universidad Tecnológica de pereira, 2019.

[32] "AUNAP | Inicio." [Online]. Available: https://www.aunap.gov.co/

[33] "María Claudia Merino Bióloga Marina Dirección Técnica de Administración y Fomento AUTORIDAD NACIONAL DE ACUICULTURA Y PESCA-AUNAP 2018 ACUICULTURA EN COLOMBIA," Tech. Rep.

[34] "Guía Práctica de Piscicultura en Colombia." [Online]. Available: https://www.aunap.gov.co/wp-content/uploads/2016/04/Guia-Practica-de-Piscicultura-en-Colombia.pdf

[35] "Solar Photovoltaic Power Potential by Country." [Online]. Available: https://www.worldbank.org/en/topic/energy/publication/solar-photovoltaic-power-potential-by-country

[36] J. S. Vélez-Ramírez, L. A. Riós-Noreña, and E. Giraldo, "Buck converter current and voltage control byexact feedback linearization with integral action," *Engineering Letters*, vol. 29, no. 1, pp. 168–176, 2021.

[37] M. H. Rashid, "Electronica de Potencia Muhammad Rashid 3º.pdf," p. 904, 2004.

[38] H. Sira-Ramírez, R. Márquez, F. Rivas-Echeverría, and O. Llanes-Santiago, *Control de Sistemas No Lineales*. Prentice Hall, 2004.

[39] Q. Lu, Y. Sun, and S. Mei, *Nonlinear Control Systems and Power System Dynamics*. Kluwer Academic Publishers, 2001.